Downregulation of the Glial GLT1 Glutamate Transporter and Purkinje Cell Dysfunction in a Mouse Model of Myotonic Dystrophy

Géraldine Sicot, Laurent Servais, Diana Dinca, Axelle M Leroy, Cynthia Prigogine, Fadia Medja, Sandra Braz, Aline Huguet-Lachon, Cerina Chhuon, Annie Nicole, et al.

Article

Cell Reports

Downregulation of the Glial GLT1 Glutamate Transporter and Purkinje Cell Dysfunction in a Mouse Model of Myotonic Dystrophy

Graphical Abstract

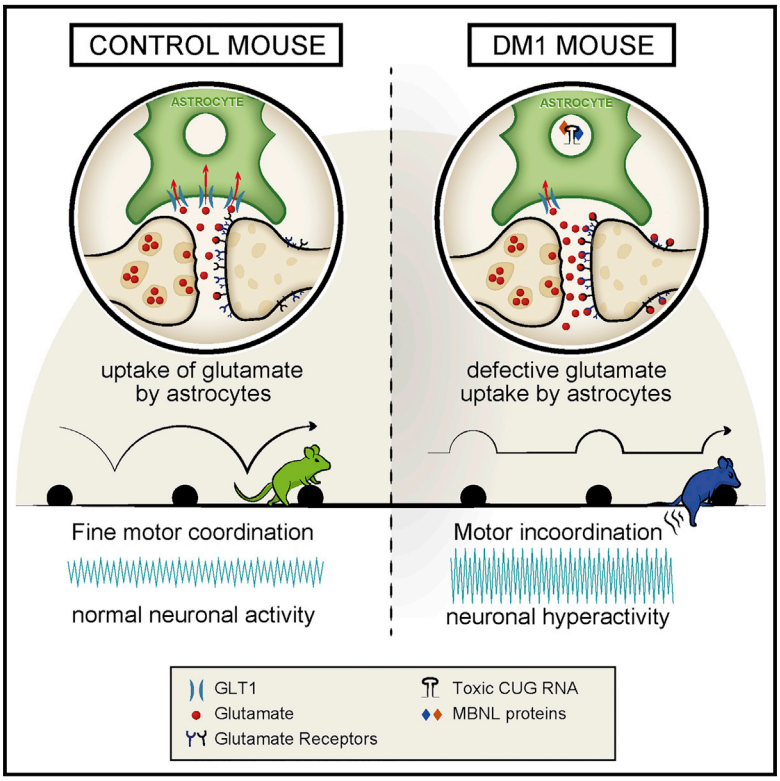

Highlights

- Bergmann glia show marked RNA toxicity in the cerebellum of DM1 mice and patients
- DM1 mice show reduced motor coordination associated with Purkinje cell hyperexcitability
- GLT1 is downregulated in astrocytes, causing glutamate neurotoxicity
- GLT1 upregulation rescues excitotoxicity, Purkinje firing, and motor coordination

Authors

Géraldine Sicot, Laurent Servais, Diana M. Dinca, ..., Guy Cheron, Geneviève Gourdon, Mário Gomes-Pereira

Correspondence

genevieve.gourdon@inserm.fr (G.G.), mario.pereira@inserm.fr (M.G.-P.)

In Brief

Neural dysfunction in myotonic dystrophy is not fully understood. Using a transgenic mouse model of the disease, Sicot et al. find electrophysiological and motor evidence for cerebellar dysfunction in association with pronounced signs of RNA toxicity in Bergmann glia. Upregulation of a defective glial-specific glutamate transporter corrects cerebellum phenotypes.

Sicot et al., 2017, Cell Reports *19*, 2718–2729
June 27, 2017
http://dx.doi.org/10.1016/j.celrep.2017.06.006

CellPress

OPEN ACCESS
CellPress

Cell Reports
Article

Downregulation of the Glial GLT1 Glutamate Transporter and Purkinje Cell Dysfunction in a Mouse Model of Myotonic Dystrophy

Géraldine Sicot,[1,2,10] Laurent Servais,[3,10] Diana M. Dinca,[1,2,10] Axelle Leroy,[4,5] Cynthia Prigogine,[4,5] Fadia Medja,[1,2] Sandra O. Braz,[1,2] Aline Huguet-Lachon,[1,2] Cerina Chhuon,[6] Annie Nicole,[1,2] Noëmy Gueriba,[1,2] Ruan Oliveira,[7] Bernard Dan,[4,8] Denis Furling,[9] Maurice S. Swanson,[7] Ida Chiara Guerrera,[6] Guy Cheron,[4,5] Geneviève Gourdon,[1,2,*] and Mário Gomes-Pereira[1,2,11,*]

[1]Laboratory *CTGDM*, Inserm UMR1163, 75015 Paris, France
[2]Institut Imagine, Université Paris Descartes-Sorbonne Paris Cité, 75015 Paris, France
[3]Institut I-Motion, Hôpital Armand Trousseau, 75012 Paris, France
[4]Laboratory of Neurophysiology and Movement Biomechanics, Université Libre de Bruxelles, 1050 Brussels, Belgium
[5]Laboratory of Electrophysiology, University of Mons, 7000 Mons, Belgium
[6]Proteomics Platform 3P5-Necker, Université Paris Descartes-Structure Fédérative de Recherche Necker, Inserm US24/CNRS UMS3633, 75014 Paris, France
[7]Department of Molecular Genetics and Microbiology, Center for NeuroGenetics and the Genetics Institute, University of Florida College of Medicine, Gainesville, FL 32610, USA
[8]Inkendaal Rehabilitation Hospital, Vlezenbeek B-1602, Belgium
[9]Sorbonne Universités UPMC Université Paris 06, Inserm, Centre de Recherche en Myologie UMRS974, Institut de Myologie, Groupe Hospitalier Pitié-Salpêtrière, 75013 Paris, France
[10]These authors contributed equally
[11]Lead Contact
*Correspondence: genevieve.gourdon@inserm.fr (G.G.), mario.pereira@inserm.fr (M.G.-P.)
http://dx.doi.org/10.1016/j.celrep.2017.06.006

SUMMARY

Brain function is compromised in myotonic dystrophy type 1 (DM1), but the underlying mechanisms are not fully understood. To gain insight into the cellular and molecular pathways primarily affected, we studied a mouse model of DM1 and brains of adult patients. We found pronounced RNA toxicity in the Bergmann glia of the cerebellum, in association with abnormal Purkinje cell firing and fine motor incoordination in DM1 mice. A global proteomics approach revealed downregulation of the GLT1 glutamate transporter in DM1 mice and human patients, which we found to be the result of MBNL1 inactivation. GLT1 downregulation in DM1 astrocytes increases glutamate neurotoxicity and is detrimental to neurons. Finally, we demonstrated that the upregulation of GLT1 corrected Purkinje cell firing and motor incoordination in DM1 mice. Our findings show that glial defects are critical in DM1 brain pathophysiology and open promising therapeutic perspectives through the modulation of glutamate levels.

INTRODUCTION

Repeat-containing RNA can cause neurological diseases through a *trans*-dominant gain of function (Mohan et al., 2014; Sicot and Gomes-Pereira, 2013). RNA toxicity is best described in myotonic dystrophy type 1 (DM1), but it operates in an increasing number of conditions (Sicot et al., 2011). DM1 is the most common muscular dystrophy in adults, with a variable prevalence ranging from 0.5 to 18 cases in 100,000 individuals (Theadom et al., 2014). DM1 is a multisystemic disorder that affects the skeletal muscle, heart, and the CNS, among other tissues (Udd and Krahe, 2012). Five main clinical forms of DM1 can be distinguished based on age at onset: congenital, childhood, juvenile, adult, and mild or late onset (Dogan et al., 2016). CNS impairment is more pronounced in the early-onset cases. Among these, the congenital patients exhibit moderate to severe intellectual disability. The childhood- and juvenile-onset cases can also show reduced IQ, low cognitive processing speed, and visuospatial impairment, as well as attention and executive deficits (Angeard et al., 2007, 2011). The main CNS manifestations in the adult form include dysexecutive behavior (such as apathy, lack of motivation, and inflexibility), reduced attention and visuospatial construction ability, daytime sleepiness, and impaired social cognition (Meola and Sansone, 2007; Serra et al., 2016; Sistiaga et al., 2010). Overall, the quality of life of DM1 patients is significantly impaired by their cognitive deficits (Antonini et al., 2006; Dogan et al., 2016). Brain disease is further supported by histopathological changes, such as the aggregation of hyperphosphorylated Tau protein isoforms, particularly in the amygdala, hippocampus, and entorhinal and temporal cortex (Caillet-Boudin et al., 2014). White matter lesions, gray matter changes, metabolic deficits, and changes in functional connectivity were reported in multiple brain areas (Caliandro et al., 2013; Minnerop et al., 2011; Serra et al.,

2014, 2015; Weber et al., 2010; Wozniak et al., 2014), implicating the dysregulation of complex brain networks and various cell types (Schneider-Gold et al., 2015; Serra et al., 2016). However, the link between the distribution of DM1 pathology across brain territories and cell types and the neurological symptoms of the disease must be further elucidated.

DM1 is caused by the expansion of an unstable CTG repeat in the 3′ untranslated region (3′ UTR) of the DM protein kinase (*DMPK*) gene (Brook et al., 1992). Repeat number correlates with disease severity and inversely with age of onset. Expanded *DMPK* transcripts accumulate in nuclear RNA foci and perturb the activity of multiple RNA-binding proteins. Among these, the sequestration of muscleblind-like (MBNL) proteins and the upregulation of the CUGBP/Elav-like family (CELF) affect primarily alternative splicing but also RNA transcription, localization and polyadenylation, miRNA processing, protein translation, and phosphorylation of downstream targets (Batra et al., 2014; Goodwin et al., 2015; Hernández-Hernández et al., 2013a, 2013b; Sicot et al., 2011; Wang et al., 2012). Today we do not know the extent or distribution of these events in the CNS, their cellular specificity, or how they contribute to neuropathogenesis.

To investigate DM1 brain disease, we have been using DMSXL mice, which carry a human *DMPK* transgene containing >1,000 CTG repeats (Gomes-Pereira et al., 2007; Seznec et al., 2000). DMSXL homozygotes express enough toxic transcripts to perturb muscular, cardiac, and respiratory function (Algalarrondo et al., 2015; Huguet et al., 2012; Panaite et al., 2013), in association with RNA foci and missplicing (Hernández-Hernández et al., 2013a; Huguet et al., 2012). The expression of expanded CUG RNA in the CNS affects behavior and synaptic function of DMSXL mice (Hernández-Hernández et al., 2013a). In contrast, DM20 mice, overexpressing short *DMPK* transcripts, do not show RNA foci accumulation, obvious phenotypes, or synaptic protein dysfunction (Hernández-Hernández et al., 2013a; Seznec et al., 2001). The differences between mouse lines corroborate the toxicity of expanded CUG RNA repeats in the CNS of DMSXL mice. However, the underlying molecular and cellular mechanisms leading to brain impairment are not entirely known, which delays the development of efficient therapeutic strategies in the CNS.

To overcome this limitation, we have combined molecular, electrophysiological, and behavioral approaches to gain insight into the susceptible cell populations, dysfunctional connections, and affected molecular pathways in the CNS of DM1. It was our aim to better understand brain disease pathogenesis and find promising therapeutic targets. We found evidence of cerebellar glial dysfunction, which is caused by the downregulation of a glutamate transporter that affects neuronal physiology.

RESULTS

Bergmann Glia Show Abundant RNA Accumulation in DMSXL Cerebellum

To investigate the impact of the DM1 expansion on different cell populations and networks in the CNS, we investigated the distribution of the canonical molecular signs of the disease (the toxic CUG RNA foci) in different areas of the DMSXL mouse brain. We were particularly intrigued by the distinctive and peculiar distribution of RNA foci in the cerebellum. The cerebellum is a well-organized brain region with a highly specific and uniform laminar arrangement of cells into distinct, easily identified anatomical layers (Voogd and Glickstein, 1998). Fluorescence in situ hybridization (FISH) revealed that CUG RNA foci were rarely found in Purkinje cells, but in contrast, they were abundant in a population of neighboring cells, extending toward the molecular layer. MBNL1 and MBNL2 co-localized with RNA in these foci-rich cells in DMSXL mice (Figure 1A), in contrast to wild-type animals (Figure S1A). MBNL proteins remained distributed throughout the nucleus and cytoplasm of DMSXL Purkinje cells, even in those rare neurons showing RNA foci accumulation, without pronounced sequestration (Figure 1A).

Given the intriguing distribution of RNA foci in DMSXL cerebellum, we sought to identify the nature of foci-rich cells through immunodetection of cell-specific markers. NeuN stains almost exclusively mature granular neurons, whereas Fox1 and Fox2 stain Purkinje and Golgi cells; Fox2 stains also the granular neurons (Kim et al., 2011). We found that foci accumulated preferentially in non-neuronal cells of the molecular layer, which did not express NeuN, Fox1, or Fox2. The non-neuronal nature of these cells was confirmed by GFAP staining (Figure 1B). The distinctive localization around the Purkinje cells into the molecular layer of the cerebellum, the expression of GFAP, and the lack of neuronal markers strongly suggested that the foci-rich cells were Bergmann astrocytes. We have confirmed their nature by the immunodetection of GLAST/SLC1A3, a glial glutamate transporter, which in adult mouse cerebellum is primarily expressed in Bergmann glia (Regan et al., 2007): immunofluorescence combined with FISH revealed greater GLAST expression near Purkinje cells, usually in foci-rich cells (Figure 1B).

To elucidate the reasons behind the preferential accumulation of CUG RNA foci in Bergmann glia, we quantified the levels of expanded *DMPK* transcripts in Bergmann astrocytes and Purkinje cells collected from DMSXL cerebellum by laser capture microdissection. The purity of the collected cells was controlled by RT-PCR amplification of cell-specific transcripts (Figure S1B). qRT-PCR revealed levels of toxic CUG RNA nearly three times higher in Bergmann glia than in adjacent Purkinje cells (Figure 1C). We conclude that higher transgene expression in cerebellar Bergmann glia contributes to the higher foci abundance in this cell type.

RNA Spliceopathy Is More Pronounced in the Bergmann Glia of the Cerebellum

Higher levels of CUG RNA and foci in Bergmann astrocytes predict pronounced spliceopathy in this cell type. Thus, we studied splicing defects in microdissected DMSXL Bergmann and Purkinje cells. We have previously shown that *Mbnl1* and *Mbnl2* transcripts show consistent missplicing in DMSXL mouse brains (Hernández-Hernández et al., 2013a) and serve as robust markers of spliceopathy in our mouse model. In line with our hypothesis, *Mbnl1* and *Mbnl2* splicing was significantly dysregulated in DMSXL Bergmann glia while remaining unaltered in Purkinje cells (Figure 1D). Overall, the missplicing of these transcripts was mild in the analysis of whole DMSXL cerebellum (Figure S1C), suggesting that splicing abnormalities are pronounced in Bergmann astrocytes but diluted in whole-tissue samples.

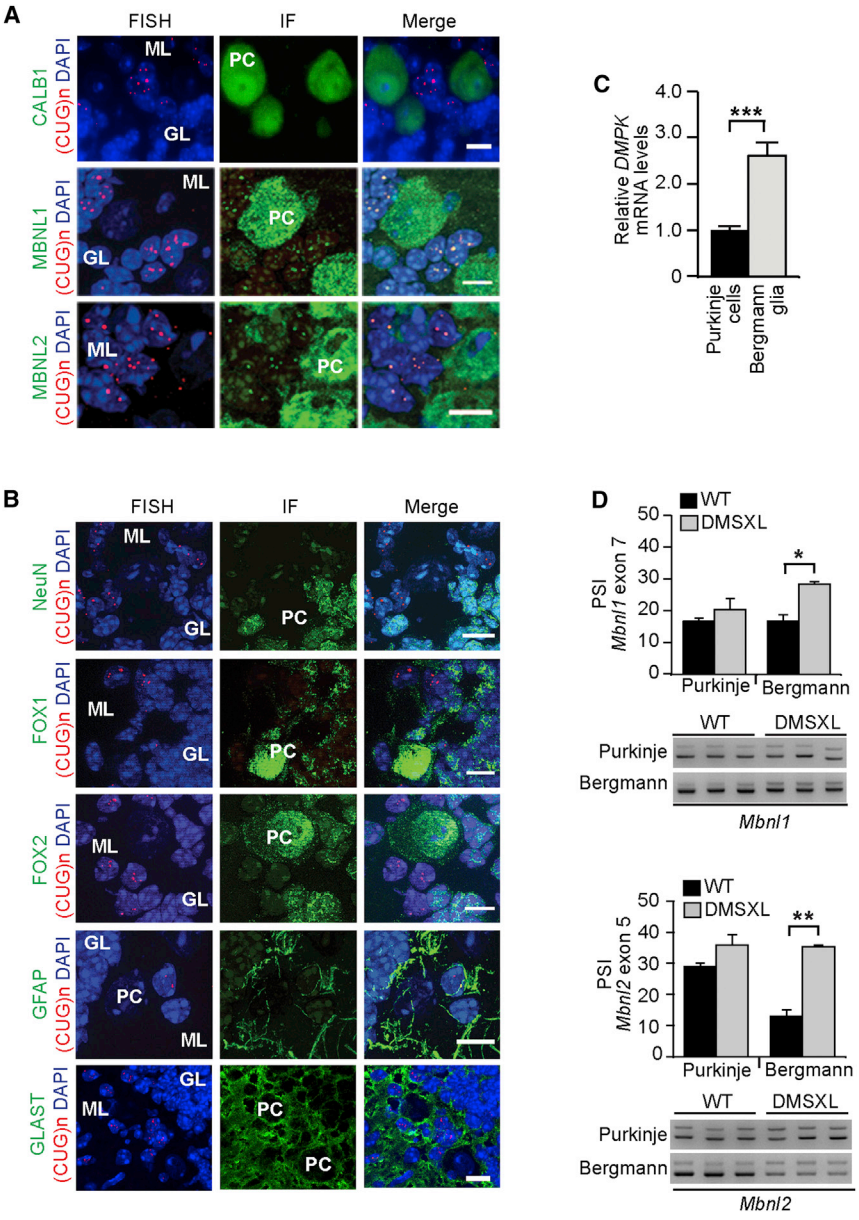

Figure 1. RNA Foci Accumulate in Cerebellar Bergmann Astrocytes and Deregulate Alternative Splicing

(A) FISH detection of RNA foci (red) and immunofluorescence of calbindin 1 (CALB1) and MBNL proteins (green) in mouse cerebellum. An example of a rare foci-positive Purkinje cell is shown in the bottom panel.

(B) Identification of cell types showing abundant nuclear RNA foci (red) in DMSXL cerebellum through immunodetection of NeuN, Fox1, Fox2, GFAP, or GLAST (green). DAPI was used for nuclear staining.

(C) Nested qRT-PCR of *DMPK* transgene expression (±SEM) in Purkinje cells and Bergmann astrocytes microdissected from DMSXL cerebellum (n = 3).

(D) Percent of spliced in (PSI) of alternative exon 7 of *Mbnl1* and exon 5 of *Mbnl2* transcripts (±SEM). Purkinje cells and neighboring Bergmann glia were collected by laser microdissection from DMSXL and wild-type (WT) mice (n = 3, each genotype). Three independent technical replicates were studied for each mouse. Representative analyses of alternative splicing by nested RT-PCR are shown.

PC, Purkinje cells; GL, granular layer; ML, molecular layer. The scale bar represents 10 μm. $^{*}p < 0.05$, $^{**}p < 0.01$, $^{***}p < 0.001$; Mann-Whitney U test. See also Figure S1.

Finally, we assessed the contributing role of CELF proteins to cerebellum pathology. Western blot analysis in whole DMSXL cerebellum revealed mild upregulation of CELF2 but no significant changes in CELF1 levels (Figure S1D).

Electrophysiological Abnormalities of Purkinje Cells in DMSXL Cerebellum

We next investigated whether Bergmann RNA toxicity in DMSXL mice was sufficient to affect cerebellar function. The functional output of the cerebellar cortex is determined by the Purkinje cell firing, which can be electrophysiologically identified by two types of firing patterns: complex spikes and simple spikes (Cheron et al., 2013). We performed electrophysiological recordings in the Purkinje cell layer of alert DMSXL mice and found significantly higher simple spike firing rates (86.8 ± 7.6 versus 50.5 ± 4.2 Hz) and rhythmicity index (0.13 ± 0.02 versus 0.07 ± 0.01) in DMSXL mice relative to the wild-type controls, indicative of neuronal hyperactivity of Purkinje cells (Figure 2A). In addition, spontaneous fast local field potential (LFP) oscillations were found throughout the cerebellum in all DMSXL mice but were absent in wild-type controls. DMSXL fast LFP oscillations appeared as spindle-shaped episodes of oscillation with a frequency of 200 ± 27 Hz and maximal amplitude of 0.48 ± 0.26 mV (Figure 2B). We quantified calcium buffering proteins and studied DMSXL cerebellum histology, but we did not find obvious changes in steady-state protein levels or overt histopathology that could contribute to the defective Purkinje neuronal activity and cerebellum dysfunction (Figures S2A and S2B).

Cerebellum-Dependent Motor Incoordination in DMSXL Mice

To confirm cerebellar dysfunction in DMSXL mice, we assessed a cerebellum-dependent behavior phenotype. In the runway test, mice run along an elevated platform and must surmount low obstacles intended to impede their progress. The test assesses cerebellum-dependent motor coordination, and in contrast with rotarod, it is minimally influenced by muscle

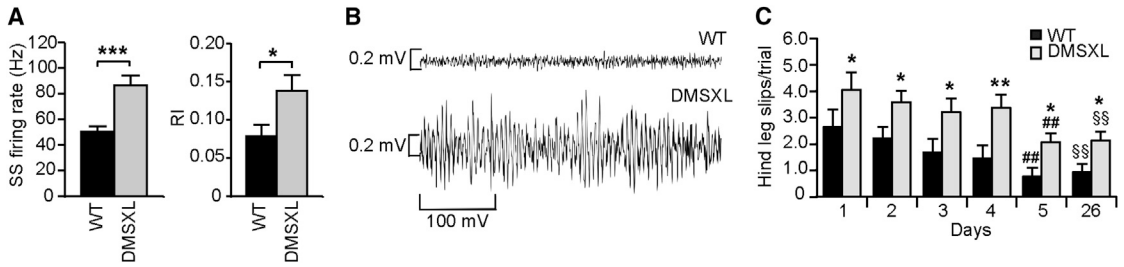

Figure 2. Cerebellum Dysfunction in DMSXL Mice Revealed by Behavioral and Electrophysiological Phenotyping

(A) In vivo electrophysiological recordings of single spike (SS) frequency and rhythmicity index (RI) in 2-month-old alert DMSXL (n = 4) and WT mice (n = 3). Error bars represent the SEM. *p < 0.05, ***p < 0.001; Mann-Whitney U test.

(B) Representative fast LFP oscillation in the cerebellum of one DMSXL compared to WT control.

(C) Assessment of cerebellum-dependent motor-coordination of DMSXL (n = 20) and WT controls (n = 21), at 3–4 months in the runway test over 5 consecutive days (days 1–5). The graph represents the average number of hind leg slips per trial (±SEM) (*p < 0.05, **p < 0.01; two-way ANOVA). Learning was assessed by the number of slips at day 5 relative to day 1 (##p < 0.01; two-way ANOVA). Retention of the task was assessed at day 26, following a period of 3 weeks without testing, relative to day 1 (§§p < 0.01; two-way ANOVA).

See also Figure S2.

performance (Bearzatto et al., 2005). The number of slips of the right hind leg is a direct indication of motor incoordination.

Both wild-type and DMSXL showed a progressive and significant decrease in number of hind leg slips from day 1 to day 5 (Figure 2C), indicating the capacity to learn new cerebellum-dependent tasks. However, DMSXL mice showed significantly higher numbers of slips from day 1, pointing to deficits in the fine-tuning of movements and cerebellar dysfunction. After 3 weeks, the test still revealed significantly lower number of slips relative to day 1 in both wild-type and DMSXL mice, demonstrating efficient task retention by both genotypes (Figure 2C). In summary, although capable of acquiring and retaining new cerebellum-dependent motor tasks, DMSXL mice showed signs of motor incoordination.

In conclusion, both electrophysiological and behavioral assessment demonstrated that the expression and accumulation of toxic RNA foci in DMSXL cerebellum (particularly in Bergmann glia) are associated with cerebellum pathology, which is characterized by abnormal Purkinje cell firing and fine motor incoordination.

The GLT1 Glutamate Transporter Is Downregulated in DMSXL Cerebellum

To decipher the mechanisms of abnormal Purkinje cell activity and cerebellar dysfunction, we used global proteomics to identify expression changes and dysregulated pathways in DMSXL cerebellum. We first studied whole-cell lysates and found that the expression of 241 proteins was altered in DMSXL cerebellum. A Gene Ontology analysis on this 241-protein set revealed that many altered proteins were membrane-bound, but we did not find a biological process predominantly dysregulated in DMSXL cerebellum (Figure 3A). To refine our search, we specifically investigated the membrane-bound proteome of mouse cerebellum and found 60 proteins with altered expression in DMSXL cerebellum. This protein set showed enrichment for ion transport, synaptic transmission, and glutamate signaling (Figure 3B) and included the glial high-affinity glutamate transporter (GLT1) (excitatory amino acid transporter 2 [EAAT2] or solute carrier family 1 member 2 [SLC1A2]). GLT1 is a membrane transporter that in the cerebellum is mainly expressed by the Bergmann glia to clear glutamate released during synaptic transmission from the extracellular space, avoiding excessive stimulation of postsynaptic neurons (Kanai and Hediger, 2004). Therefore, we tested the hypothesis that abnormal GLT1 expression in DMSXL cerebellum results in defective neuroglial communication and abnormal DMSXL Purkinje cell firing.

We first confirmed GLT1 downregulation by western blot in DMSXL cerebellum (Figure 3C), as well as in other mouse brain regions (Figure S3A), but not in control DM20 mice (Figure S3B). Semiquantitative analysis of GLT1 immunofluorescence intensity by confocal microscopy showed a significant reduction in the DMSXL molecular layer, close to the Purkinje cells (Figure S3C). In contrast to GLT1, the levels of GLAST remained unchanged in DMSXL brains (Figure S3D), demonstrating that the impact of expanded *DMPK* transcripts is specific to the GLT1 glutamate transporter. Fractioning of DMSXL cerebellar tissue revealed downregulation of GLT1 in the membrane-bound protein faction (Figure 3D), in line with defective glutamate transport across the membrane. To investigate the functional impact of reduced GLT1 levels, we measured the uptake of radioactive glutamate by DMSXL astrocytes in the presence of WAY213623 (GLT1-specific inhibitor), UCPH (GLAST-specific inhibitor), or TBOA (pan-glutamate transporter inhibitor). We found a significant reduction in total and in GLT1-mediated glutamate uptake when compared to wild-type controls (Figure 3E), consistent with GLT1 downregulation in DMSXL astrocytes (Figure S3E). In contrast, GLAST-mediated transport was unaltered, while TBOA nearly abolished glutamate uptake in both cultures. Transfection of DMSXL astrocytes with GLT1-expressing plasmids corrected defective glutamate transport (Figure 3E). Altogether, these results demonstrate the causative role of GLT1 downregulation in defective glutamate transport by DMSXL astrocytes. GLT1 downregulation is not explained by Bergmann cell loss, as revealed by the quantification of Bergmann-specific transcripts in DMSXL cerebellum, which showed no reduced expression relative to wild-type controls (Figure S3F). Overall, the reduction of GLT1 within the molecular layer is consistent with Bergmann dysfunction.

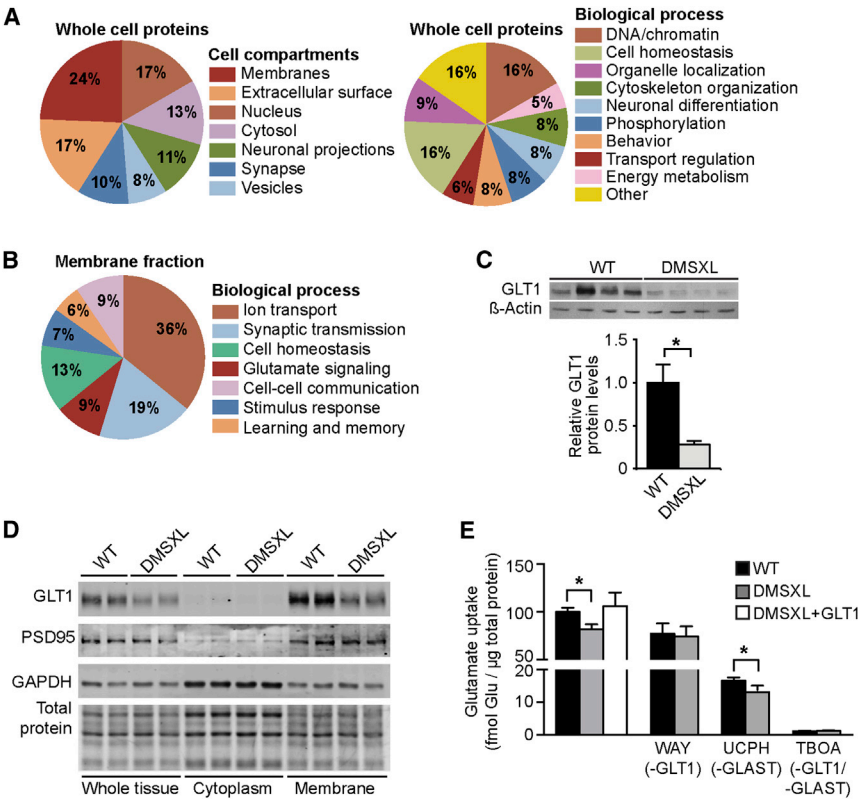

Figure 3. GLT1 Downregulation in DMSXL Cerebellum

(A) Isobaric tag for relative and absolute quantification (iTRAQ) analysis of whole cell protein fractions collected from the cerebellum of 2-month-old DMSXL mice and WT littermates (n = 4, each genotype). Pie charts indicate the percentage of altered proteins in the cellular components and biological processes showing the highest significant enrichment in the proteomics expression data.

(B) Quantitative proteomics analysis of the membrane-bound proteins from the cerebellum of 2-month-old DMSXL mice and WT littermates (n = 2, each genotype). Pie charts indicate the percentage of altered membrane proteins in the biological processes showing the highest significant enrichment.

(C) Western blot quantification of GLT1 protein levels in the cerebellum of DMSXL and WT mice (n = 4, each genotype) at 2 months of age. β-actin was used as loading control.

(D) Western blot detection of GLT1 in cytosolic and membrane protein fractions of DMSXL and WT cerebellum at 2 months of age (n = 2, each genotype). GAPDH and PSD95 confirmed cytosolic and membrane protein enrichment, respectively. Total protein was visualized by stain-free protocols and used as loading control.

(E) Uptake of radioactive glutamate by WT and DMSXL astrocytes: under control conditions, following DMSXL transfection with GLT1-expressing plasmids, or upon selective inhibition of GLT1 (WAY213623), GLAST (UCPH 101), or both (TBOA) (n = 3, each group).

Errors bars represent the SEM. *p < 0.05; Mann-Whitney U test. See also Figure S3.

Human DM1 Cerebellum Shows Bergmann-Specific RNA Foci Accumulation and GLT1 Downregulation

We then assessed the implications of the mouse findings to the human condition through the analysis of post-mortem DM1 brains. In human DM1 cerebellum, although small foci were rarely detected in Purkinje cells, large and more abundant foci accumulated predominantly in calbindin 1 (CALB1)-negative cells, co-localizing with MBNL1 and MBNL2 (Figure 4A). Like in DMSXL mice, the preferential accumulation of RNA foci was concentrated in the Bergmann glia, which expressed GFAP and GLAST in the absence of NeuN, Fox1, or Fox2 neuronal markers (Figure 4B). The analysis of selected MBNL1 and MBNL2 candidate splicing events revealed that human DM1 cerebellar tissue showed mild spliceopathy (Figure S4A), in association with CELF2 upregulation (Figure S4B).

Finally, we studied GLT1 protein expression in human DM1 cerebellum and found a dramatic reduction in five of seven adult DM1 patients: overall, GLT1 was reduced by ~50% relative to non-DM controls (Figure 4C). GLT1 was also decreased in DM1 frontal cortex and brainstem (Figure S4C), indicating wider dysregulation of this glutamate transporter throughout the CNS.

GLT1 Downregulation Is Mediated by MBNL1 Inactivation

To gain insight into the mechanisms of GLT1 downregulation, we quantified transcript levels and found significantly lower levels of *GLT1* mRNA in the cerebellum and frontal cortex of the DM1 patients with pronounced protein downregulation (Figure 5A). In amyotrophic lateral sclerosis (ALS), missplicing of *GLT1* results in RNA degradation and loss of protein (Lin et al., 1998). To test whether similar mechanisms operate in DM1, we studied ALS-associated exon missplicing and abnormal intron retention. We did not find obvious splicing abnormalities in DM1 patients or in DMSXL mice (Figures 5SA and 5SB).

We then tested whether GLT1 downregulation was the direct result of the expression of CUG-containing RNA or a secondary consequence associated with DM1 brain disease progression. To this end, we transfected human T98G glioblastoma cells with expanded *DMPK* constructs and found that CUG RNA expansions reduced *GLT1* transcript levels relative to no-repeat control constructs (Figure 5B).

MBNL proteins regulate various aspects of RNA metabolism. Hence, we tested whether MBNL1 or MBNL2 inactivation was sufficient to lower GLT1 levels. We used short hairpin RNA (shRNA) to knockdown MBNL1 and/or MBNL2 in T98G cells (Figure S5C). qRT-PCR revealed that MBNL1 downregulation alone was sufficient to decrease *GLT1* mRNA levels, while MBNL2 inactivation left *GLT1* transcripts unchanged (Figure 5C). The simultaneous treatment with MBNL1 and MBNL2 shRNA resulted in a modest downregulation of both MBNL proteins (Figure S5C), which was insufficient to affect *GLT1* mRNA levels. We confirmed the determinant role of MBNL1 in vivo through

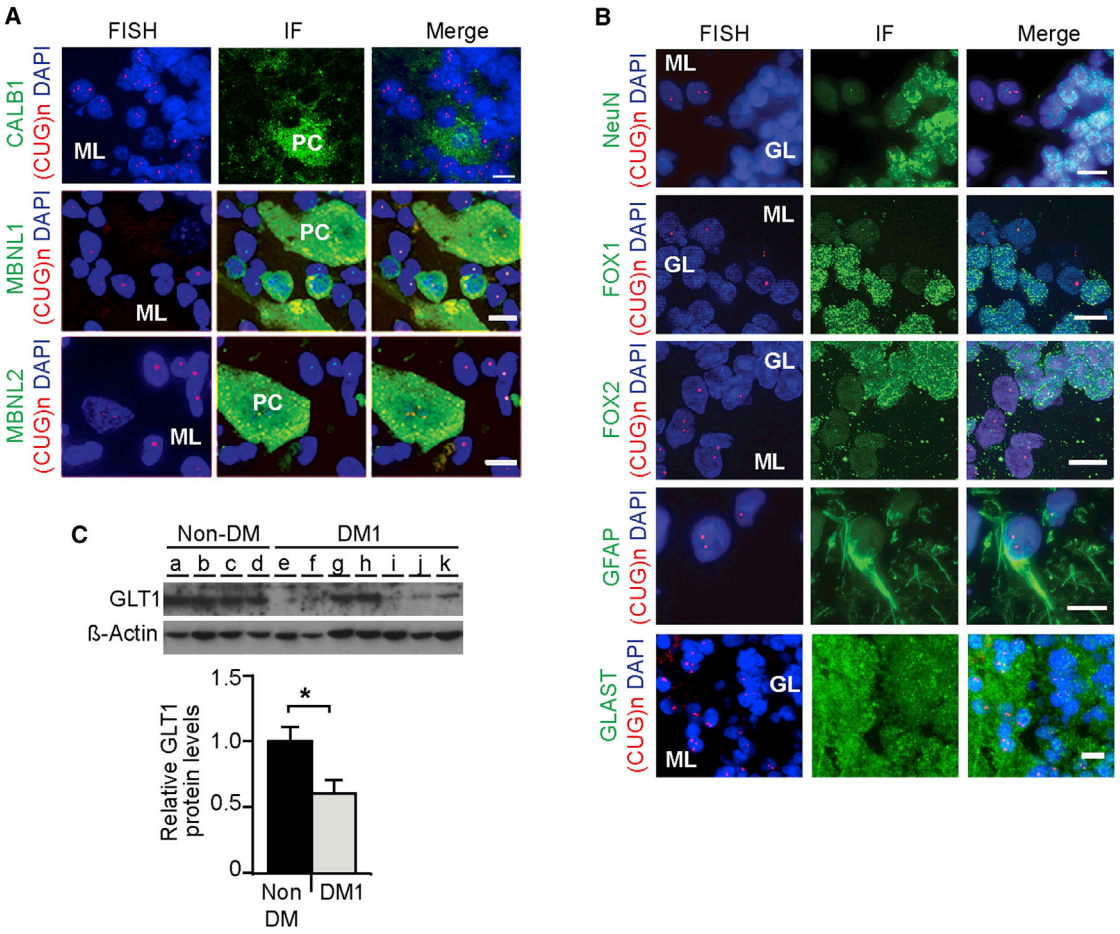

Figure 4. Analysis of RNA Foci Accumulation and GLT1 Downregulation in Human DM1 Cerebellum

(A) FISH of RNA foci (red) combined with immunofluorescence detection of CALB1 and MBNL proteins (green) in post-mortem brains from adult DM1 patients. Some rare and small RNA foci were detected in human Purkinje cells but were not associated with pronounced sequestration of MBNL proteins.

(B) FISH of RNA foci (red) and protein markers (green) of different cerebellar cell populations near Purkinje cells.

(C) Western blot quantification of GLT1 in DM1 cerebellum (n = 7) relative to non-DM controls (n = 4). β-actin was used as loading control.

The scale bar represents 10 μm. Error bars represent the SEM. *p < 0.05; Mann-Whitney U test. See also Figure S4.

the analysis of *Mbnl1* and *Mbnl2* knockout (KO) mice (Charizanis et al., 2012; Kanadia et al., 2003): only the cerebellum of *Mbnl1*$^{-/-}$ mice showed significant downregulation of GLT1. In contrast to double-shRNA-transfected T98G cells, the inactivation of MBNL1 and MBNL2 proteins in *Mbnl1*/*Mbnl2* double-KO mice (Goodwin et al., 2015) significantly reduced GLT1 levels (Figures 5D and S5D).

In an attempt to provide insight into the prevalent role of MBNL1 over MBNL2 in the regulation of the glial-specific GLT1 glutamate transporter, we quantified the expression of MBNL proteins in mouse primary neurons and astrocytes. The analysis revealed that the relative expression of MBNL1 is 2-fold higher in mouse primary astrocytes relative to neurons (Figure S5E), suggesting a more important role of MBNL1 in glial cells.

Because CELF2 is upregulated in DM1 brains, we also studied whether CELF proteins could regulate GLT1 expression and contribute to abnormal GLT1 levels. Transient transfection of CELF1 and CELF2 in T98G cells (Figure S5F) did not result in lower *GLT1* mRNA levels (Figure 5E).

In summary, our results demonstrate that GLT1 protein downregulation in DM1 is associated with lower transcript levels without evidence of missplicing and is mediated by partial inactivation of MBNL1 in glial cells, independently of CELF proteins.

GLT1 Downregulation in DMSXL Astrocytes Is Associated with Increased Glutamate Neurotoxicity

Glutamate transporters guard against prolonged elevation of extracellular glutamate concentration and protect neurons from excitotoxicity (Kanai and Hediger, 2004). To investigate the impact of GLT1 downregulation on neuronal physiology in DM1, we tested whether primary DMSXL astrocytes expressing significantly lower levels of GLT1 (Figure S3E) failed to protect neurons against glutamate neurotoxicity in culture. To this end, we co-cultured neurons and astrocytes of mixed genotypes and allowed neurites to extend for 8 days. Then, we added 50 μM of glutamate to the medium and monitored neuronal damage by measuring neurite collapse by fluorescence live-cell videomicroscopy (Figure 6A). Neurite collapse was significantly

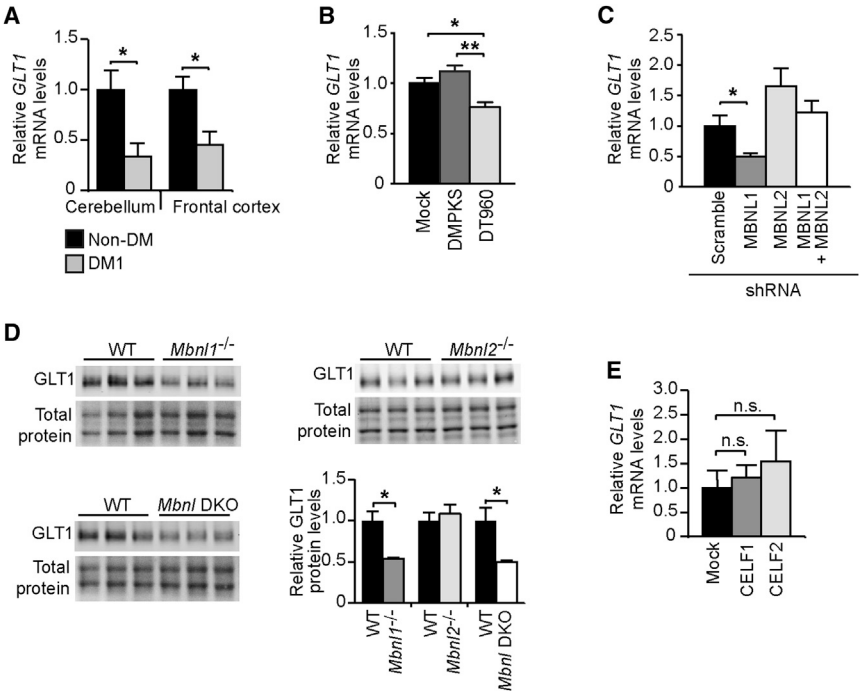

Figure 5. Transcriptional *GLT1* Downregulation Is Mediated by MBNL1 Inactivation

(A) Quantification of *GLT1* transcripts (±SEM) in the cerebellum and frontal cortex of DM1 patients showing the most pronounced protein decrease (n = 5) relative to non-DM controls (n = 4).

(B) Quantification of *GLT1* transcripts in human T98G glial cells transfected with expanded *DMPK* constructs containing 960 interrupted CTG repeats (DT960) relative to no-repeat (DMPKS) and mock transfected controls.

(C) Quantification of *GLT1* mRNA following MBNL1 and/or MBNL2 knockdown in T98G cells.

(D) Western blot quantification of GLT1 protein levels in 2- to 4-month-old *Mbnl1* KO, *Mbnl2* KO, in *Mbnl1*/*Mbnl2* double-KO mice (DKO) relative to WT littermates (n = 3, each genotype). Representative western blot membranes of at least three technical replicates. Total protein was visualized by stain-free protocols and used as loading control.

(E) Quantification of *GLT1* mRNA in T98G cells overexpressing CELF1 or CELF2.

Data are represented as the mean (±SEM) of three independent experiments in (B), (C), and (E). *p < 0.05, **p < 0.01; Mann-Whitney U test in (A) and (D), one-way ANOVA in (B) and (C); n.s., not statistically significant. See also Figure S5.

more pronounced in wild-type and DMSXL neurons co-cultured with DMSXL astrocytes than in neurons grown with wild-type astrocytes (Figure 6B). Antagonists of NMDA and AMPA receptors reduced glutamate-induced neurite collapse and eliminated differences between genotypes (Figure 6B), demonstrating the mediating role of glutamate receptors in the neurotoxicity detected in neuroglial cultures. The increased glutamate neurotoxicity in the presence of DMSXL astrocytes was not accounted for by significant changes in the expression of NMDA and AMPA receptors: western blot quantification GRIN1 (NMDA receptor subunit type 1) and GRIA2 (AMPA receptor subunit type 2) did not show significant changes in DMSXL cell cultures (Figure 6C) or in brain tissue (Figures S6A and S6B). To determine whether the deleterious effect of astrocytes on neurons was directly mediated by GLT1 downregulation, we transfected DMSXL astrocytes with GLT1 before glutamate neurotoxicity assessment. GLT1 transfection of DMSXL astrocytes rescued the neurite collapse (of both wild-type and DMSXL neurons) to levels that were indistinguishable from those measured in the presence of wild-type astrocytes (Figure 6D).

Altogether, these results demonstrate that the downregulation of GLT1 in DMSXL astrocytes perturbs the neuroglial interplay and has a negative impact on neuronal physiology, failing to protect against glutamate excitotoxicity.

GLT1 Upregulation by Ceftriaxone Corrects the Cerebellum Phenotype of DMSXL Mice

To explore the role of GLT1 downregulation in DMSXL cerebellar dysfunction, we first used LFP oscillations in the Purkinje cell layer of the cerebellar vermis to compare the extracellular electrical activity of DMSXL and *Glt1*-deficient mice, which show a ~60% reduction in GLT1 (Tanaka et al., 1997). Both DMSXL and heterozygous $Glt1^{+/-}$ mice exhibited a frequency peak of oscillations around 200 Hz, similar to wild-type controls (Figures 7A and 7B), but the amplitude of the power peak of LFP oscillations was significantly higher in $Glt1^{+/-}$ and in DMSXL mice (Figures 7C and 7D). In other words, the abnormal neuronal activity of DMSXL Purkinje cells is recreated by the partial inactivation of *Glt1*, in agreement with a mediating role of GLT1 downregulation in the onset of DMSXL cerebellar phenotypes.

To further demonstrate the implications of GLT1 in DMSXL cerebellar dysfunction, we injected DMSXL animals with ceftriaxone for 5 consecutive days. Ceftriaxone is a β-lactam antibiotic that activates GLT1 expression (Rothstein et al., 2005). Ceftriaxone corrected GLT1 protein levels in DMSXL cerebellum (Figure S7A) and glutamate neurotoxicity in DMSXL neuroglial co-cultures (Figure 6D). LFP oscillations were recorded in the same animal before and following ceftriaxone treatment. Ceftriaxone did not change the frequency peak of LFP oscillations in DMSXL mice (Figure 7B) but resulted in a remarkable reduction in the amplitude of the power peak of $Glt1^{+/-}$ and DMSXL Purkinje LFP oscillations down to wild-type values (Figures 7C and 7D). In contrast, Purkinje LFP oscillations did not change significantly in sham-treated DMSXL mice.

Finally, we assessed whether ceftriaxone-induced GLT1 upregulation (Figure S7A) ameliorated DMSXL motor coordination. A 5-day regimen of ceftriaxone significantly reduced the average number of hind leg slips from day 1 relative to PBS-injected DMSXL controls (Figure 7E). From day 2, the number of slips of ceftriaxone-treated DMSXL mice was indistinguishable from wild-type controls. To investigate whether improved Purkinje cell firing and mouse motor performance could be mediated by an effect of ceftriaxone on transgene expression, we measured *DMPK* transcripts following treatment, but we did not find

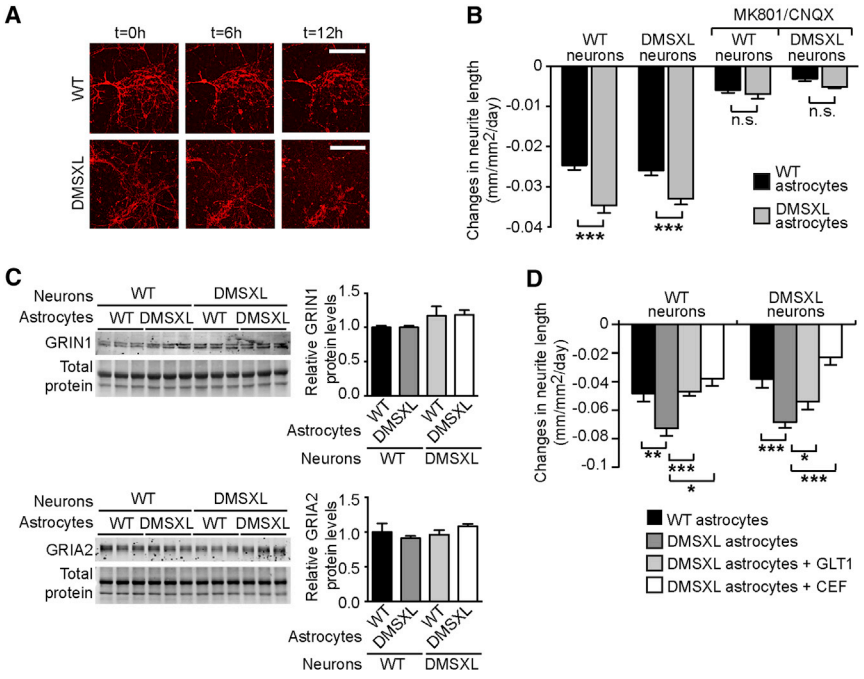

Figure 6. Neuronal Glutamate Toxicity in Mixed Cultures of Neurons and Astrocytes

(A) Representative images of WT neurite collapse co-cultured with WT and DMSXL astrocytes. Glutamate (50 μM) was added to the medium at t = 0 hr, and neurite length was monitored by the expression of fluorescent red mKate2 protein under the control of the neuron-specific synapsin-1 promoter. The scale bar represents 200 μm.

(B) Rate of glutamate-induced neurite collapse of WT and DMSXL primary neurons, cultured with WT or DMSXL astrocytes. (+)-MK 801 (NMDA receptor antagonist) and CNQX (AMPA receptor antagonist) were added to block glutamate receptors (n = 4 independent co-cultures, each mixed genotype combination). The graph shows the quantification of three independent experiments (±SEM).

(C) Representative western blot of GRIN1 (NMDA receptor subunit) and GRIA2 (AMPA receptor subunit) in mixed neuroglial cultures (n = 3 independent mixed cultures). Data are represented as the mean (±SEM). Total protein was visualized by stain-free protocols and used as loading control.

(D) Rate of glutamate-induced neurite collapse of WT and DMSXL neurons. Mouse primary neurons were cultured with WT astrocytes, control DMSXL astrocytes, DMSXL astrocytes transfected with GLT1, or DMSXL astrocytes treated with 10 μM ceftriaxone (CEF) (n = 4 independent co-cultures, each combination).

Error bars represent the SEM. *p < 0.05, **p < 0.01, ***p < 0.001; one way-ANOVA; n.s., not statistically significant. See also Figure S6.

differences relative to PBS-injected DMSXL controls (Figure S7B). Overall, these results demonstrate that reduced GLT1 is a critical contributing factor to DMSXL cerebellar pathophysiology, which can be rescued by ceftriaxone-induced upregulation of this glutamate transporter.

DISCUSSION

We found prevalent signs of RNA toxicity in the Bergmann glia of a mouse model of DM1, in association with cerebellar abnormalities, such as network-mediated Purkinje cell excitability and motor incoordination. We demonstrated that defective expression of GLT1 glutamate transporter in astrocytes plays a determinant role in mediating these phenotypes.

Bergmann glia consist of a population of astrocytes whose cell bodies are embedded in the Purkinje layer. Their cellular processes create a microenvironment essential for the good functioning of the Purkinje synapses (Bellamy, 2006). Purkinje cells are the sole output of the cerebellar cortex. Their firing is an integrated response to their intrinsic excitability and to the excitatory and inhibitory inputs from the cerebellar network (Cheron et al., 2013). Thus, the electrophysiological recordings of spontaneous firing rate and rhythmicity in vivo provide an efficient way of assessing the functional states of the cerebellar neuronal network, independently of confounding factors, such as the muscle pathology and the reduced body weight of DMSXL mice (Gomes-Pereira et al., 2007; Huguet et al., 2012). Hence, the fast LFP oscillations registered in DMSXL mice revealed pathological changes in integrated Purkinje cell activity (Cheron et al., 2008), which may result from the synchronization of high-frequency rhythmic firing caused by intrinsic Purkinje cell excitability (Cheron et al., 2004), granular cell hyperexcitability (Bearzatto et al., 2006; Cheron et al., 2004), or altered synaptic plasticity (Servais et al., 2007). Abnormal spontaneous fast LFP oscillations were previously reported in ataxic mice showing cerebellum-dependent motor incoordination (Bearzatto et al., 2006; Cheron et al., 2004, 2005; Servais et al., 2007), supporting their contribution to the motor phenotype of DMSXL mice in the runway test. In contrast, other patterns of abnormal firing, such as slow firing (Servais and Cheron, 2005) or bursting (Cheron et al., 2009), were associated with milder or more severe incoordination, respectively.

Despite their functional abnormalities, Purkinje cells did not display abundant RNA foci or pronounced missplicing in DMSXL mice, hinting that neuronal hyperactivity is not mediated by an autonomous *trans*-dominant effect of CUG repeats operating in Purkinje cells alone. Our data suggest that *DMPK* transcript levels in Purkinje cells are insufficient to trigger RNA foci accumulation and toxicity. We propose that Purkinje cell hyperexcitation is mediated by abnormalities in the neighboring Bergmann glia, which show high *DMPK* expression and abundant RNA foci, in association with GLT1 downregulation.

GLT1 is a glial-specific glutamate transporter that recaptures excitatory glutamate from the synaptic cleft and protects from neurotoxicity due to excessive glutamate stimulation (Bellamy, 2006). The most important role of the glial glutamate transporters in the cerebellum is to avoid neurotransmitter spillover and activation of extra-synaptic receptors, thereby maintaining synapse independence. In the cerebellum, Bergmann astrocytes closely appose Purkinje cells, dictating a robust effect of GLT1 on

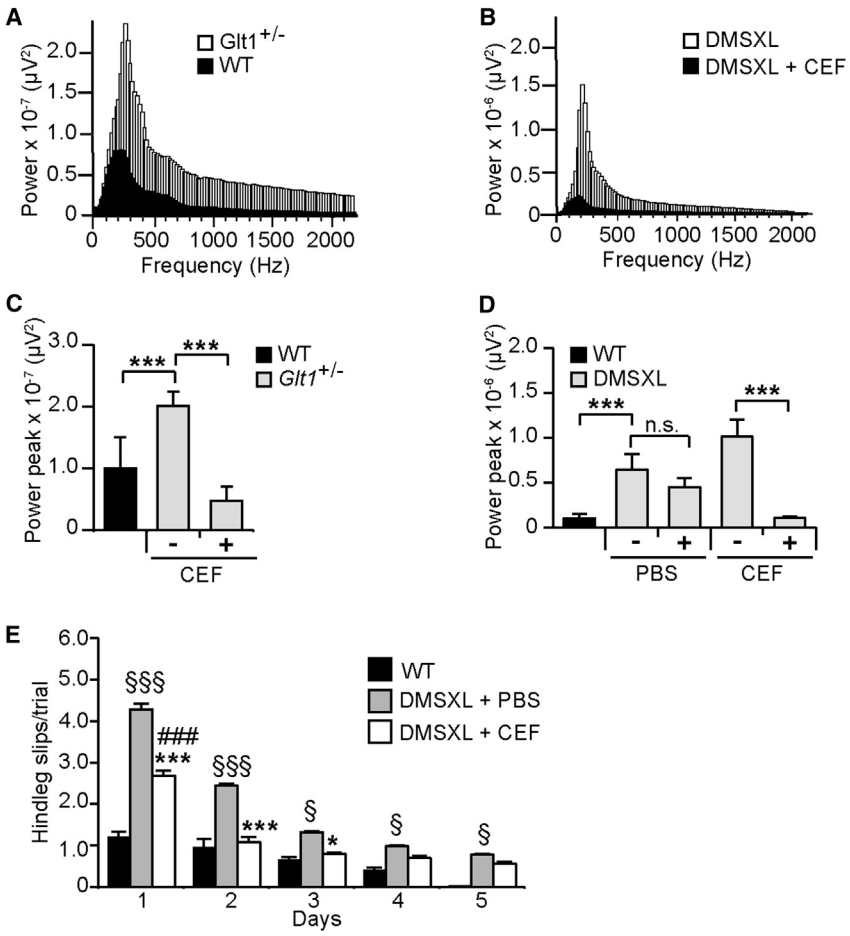

Figure 7. Rescuing of DMSXL Cerebellum Phenotype following GLT1 Upregulation by Ceftriaxone

(A) Representative profiles of LFP oscillations recorded over 690 min in the Purkinje cell layer of a *Glt1*$^{+/-}$ mouse and a WT control.

(B) Representative profiles of LFP oscillations recorded over 690 min in DMSXL mice before and following ceftriaxone injection.

(C) The power peak of the LFP oscillation (±SEM) was calculated by fast Fourier transform (FFT) analysis in *Glt1*$^{+/-}$ mice (n = 4) and WT controls (n = 3). *Glt1*$^{+/-}$ LFP oscillations were assessed before and following ceftriaxone injection. ***p < 0.001; one-way ANOVA.

(D) Effect of ceftriaxone on the power peak of the LFP oscillation (±SEM) in DMSXL mice (n = 5). Control DMSXL mice were injected with PBS (n = 4). Non-injected WT mice are shown as controls (n = 3). ***p < 0.001; one-way ANOVA; n.s., not statistically significant.

(E) Runway assessment of motor coordination of DMSXL mice injected with ceftriaxone relative to control DMSXL animals injected with PBS (n = 9, each group; *p < 0.001, ***p < 0.001; two-way ANOVA). The graphs represent the mean number of hind leg slips per trial (±SEM). Ceftriaxone-treated animals were compared with non-treated WT controls (n = 9; ###p < 0.001 at day 1; two-way ANOVA). DMSXL mice injected with PBS performed consistently worse than WT controls throughout the entire test (§p < 0.05, §§§p < 0.001; two-way ANOVA). Mice were studied at 2 months of age.

See also Figure S7.

synaptic transmission through proximity: even small changes in the density of Bergmann GLT1 transporters have a significant impact on Purkinje cell function (Tzingounis and Wadiche, 2007). Therefore, GLT1 downregulation can lead to increased synaptic glutamate, chronic Purkinje cell hyperexcitation, and emergence of fast oscillations. The critical role of GLT1 downregulation in the cerebellar dysfunction of DMSXL mice is corroborated by two observations. First, heterozygous *Glt1*$^{+/-}$ mice show similar electrophysiological LFP abnormalities. Second, ceftriaxone-mediated GLT1 upregulation corrects the spontaneous hyperactivity of DMSXL Purkinje cells and motor incoordination. The similar benefits of ceftriaxone treatment and GLT1 transfection on neuronal physiology in co-cultures strongly point to a rescuing mechanism of ceftriaxone mediated by GLT1 upregulation. Moreover, ceftriaxone was capable of correcting the Purkinje cell activity in *Glt1*$^{+/-}$ mice, in further support of a specific effect on this target. In conclusion, the benefits of GLT1 upregulation in DMSXL neuroglial co-cultures and in mice demonstrate the role of defective neuroglial interactions in DM1 brain disease.

Inactivation of *Glt1* causes lethal spontaneous seizures in KO mice, in association with selective hippocampal neurodegeneration, but no morphological changes in the cerebellum or signs of ataxia (Tanaka et al., 1997). Heterozygous *Glt1*$^{+/-}$ mice show a ~60% reduction in GLT1 protein levels, and like DMSXL mice, they exhibit abnormally high cerebellar fast oscillations, together with mild behavioral phenotypes in the absence of neurodegeneration (Kiryk et al., 2008). Altogether, our results suggest that partial inactivation of GLT1 in DM1 is more likely associated with neuronal dysfunction than cell death. Broader neuronal hyperexcitability and dysfunction in DM1 beyond cerebellum is supported by the observation of GLT1 downregulation in multiple brain areas and by the increased susceptibility of DMSXL mice to pentylenetetrazol (PTZ)-induced seizures (Charizanis et al., 2012).

GLT1 is a highly regulated transporter, modulated by changes in RNA transcription, splicing and stability, post-translational modifications, and protein activity (Kim et al., 2011). MBNL1 inactivation alone decreased *GLT1* transcripts and protein. In contrast, MBNL2 inactivation alone did not affect GLT1 levels, maybe because of the compensating increase of MBNL1 protein levels (Batra et al., 2014; Goodwin et al., 2015; Mohan et al., 2014). It is conceivable that MBNL1, but not MBNL2, specifically regulates GLT1 expression in glial cells. In line with this view, the higher expression of MBNL1 in mouse primary astrocytes, when compared to mouse primary neurons, hints at a predominant role of MBNL1 in the regulation of glia-specific transcripts. Poly(A)-RNA sequencing revealed changes in the alternative

polyadenylation of the *GLT1* transcripts in the brain of DM1 and myotonic dystrophy type 2 (DM2) patients and in *Mbnl* double-KO mice (Goodwin et al., 2015). These data suggest that MBNL loss of function perturbs GLT1 polyadenylation, leading to altered levels of this glutamate transporter.

Deficits in GLT1 were reported in several neurological diseases, including Alzheimer's disease, Huntington's disease, ALS, and fragile X syndrome (Kim et al., 2011), but the underlying mechanisms and contribution to disease manifestations have not been fully resolved. As in our DM1 mouse model, GLT1 downregulation in mouse models of fragile X syndrome is associated with enhanced neuronal excitability (Higashimori et al., 2013). In DM1, the downregulation of GLT1 and altered glutamate levels in adult patients (Takado et al., 2015) suggest an impairment of the glutamatergic system. Regulation of GLT1 activity and extracellular glutamate may improve the homeostasis and neurotransmission in DM1 brains. Ceftriaxone, in particular, is well tolerated, permeable to the blood-brain barrier, and augments GLT1 promoter activity and glutamate uptake, but other small-molecule GLT1 activators have been described (Kong et al., 2014).

The cerebellum controls motor coordination, skilled voluntary movements, posture, and gait. The implication of the cerebellum in DM1 neuropathology has not been sufficiently studied. However, imaging studies suggest cerebellar abnormalities: brain voxel-based morphometry revealed white matter decrease (Minnerop et al., 2011), while fMRI showed altered connectivity in cerebellar regions implicated in planning of movements and motor coordination (Serra et al., 2016). The frequency of stumbles and falls in DM1 is 10-fold higher than in healthy controls (Wiles et al., 2006). Several aspects of DM1 disease biology could lead to gait difficulties, among these the weakness of the leg muscles (Hammarén et al., 2014). However, because in these studies muscular impairment was often an inclusion criterion, the results are only generalizable to muscularly impaired DM1 individuals, excluding those that show gait affection without muscle weakness. A study demonstrated limited contribution of muscle weakness to gait abnormalities in DM1 and suggested a role for sensory deficits (Bachasson et al., 2016). In line with this view, altered brain connectivity has been associated with patients' motor deficits (Toth et al., 2015). Adaptive cognitive strategies usually mitigate the risk of falls caused by muscle impairment, but they might be compromised in DM1 due to brain dysfunction. There is a need for clinical assessment of cerebellum deficits and their contribution to impaired balance and frequent stumbles and falls in DM1. The cerebellum may also participate in DM1 through non-motor functions. Cerebellar lesions can result in executive dysfunction, blunting or flattening of affect, constrictions in social interaction, and impaired spatial cognition (Schmahmann and Sherman, 1998). Defective Bergmann or Purkinje cell communication could mediate, at least partly, similar cognitive and behavioral deficits previously reported in DM1, but further studies are required.

In summary, our data provide insight into DM1 brain mechanisms and demonstrate how glial molecular abnormalities affect neuronal activity through neuroglial miscommunication. They open the route to the clinic, providing exciting therapeutic perspectives through the modulation of GLT1 levels and glutamate signaling. Therapies aiming to restore GLT1 protein and glutamate neurotransmission could have applicability in DM1.

EXPERIMENTAL PROCEDURES

Transgenic Mice

All animal experiments were conducted according to the ARRIVE guidelines (Animal Research: Reporting In Vivo Experiments). This project has been conducted with the authorization for animal experimentation No. 75 003 in the animal facility with the approval No. B 91 228 107, both delivered by Prefecture de Police and the French Veterinary Department.

Human Tissue Samples

Mouse cerebellum tissues were microdissected at different ages and stored at −80°C. Human cerebellum samples were collected from different laboratories: Dr. Yasuhiro Suzuki (Asahikawa Medical Center) and Dr. Tohru Matsuura (Okayama University). All experiments using human samples were approved by the ethics committees of the host institutions. Written informed-consent specimen use for research was obtained from all patients. Information relative to patients was previously described (Hernández-Hernández et al., 2013a) and is summarized in Tables S1 and S2.

Statistical Analysis

Statistical analyses were performed with Prism (GraphPad), SPSS (v.14.0, SPSS), Statistica (v.6.0, StatSoft), and/or Excel software. When two groups were compared, we first performed a normality test. Parametric data were compared using a two-tailed Student's t test (with equal or unequal variance, as appropriate). Non-parametric data were compared using a two-tailed Mann-Whitney U test. For one-way ANOVA, if statistical significance was achieved, we performed post-test analysis to account for multiple comparisons. Statistical significance was set at $p < 0.05$. The data are presented as mean ± SEM.

SUPPLEMENTAL INFORMATION

Supplemental Information includes Supplemental Experimental Procedures, seven figures, and seven tables and can be found with this article online at http://dx.doi.org/10.1016/j.celrep.2017.06.006.

AUTHOR CONTRIBUTIONS

Conceptualization, L.S., G.C., G.G., and M.G.-P.; Methodology, G.S., L.S., D.M.D., I.C.G., G.C., G.G., M.G.-P.; Investigation, G.S., L.S., D.M.D., A.L., C.P., S.O.B., B.D., F.M., C.C., A.H.-L., A.N., N.G., R.O., I.C.G., G.C., and M.G.-P.; Formal Analysis, G.S., L.S., D.M.D., A.L., S.O.B., B.D., F.M., I.C.G., D.F., G.C., G.G., and M.G.P.; Resources, L.S., D.F., M.S.S., I.C.G., G.C., G.G., and M.G.-P.; Writing – Original Draft, G.S., L.S., D.M.D., I.C.G., C.G., and M.G.-P.; Writing – Review and Editing, G.S., L.S., D.M.D., C.G., G.G., and M.G.-P.; Funding Acquisition, L.S., G.C., G.G., and M.G.-P.

ACKNOWLEDGMENTS

We thank Dr. Thomas Cooper for providing the DMPKS, DT960, CELF1, and CELF2 plasmids; Dr. Nicolas Reyes for the GLT1-EGFP-expressing plasmid; Dr. Rob Willemsen for FXTAS mouse brain slices; and Dr. Jeffrey Rothstein for anti-GLT1 antibody. We are grateful to the personnel of CERFE (Centre d'Exploration et de Recherche Fonctionelle Expérimentale, Genopole, Evry, France) and LEAT (Laboratoire d'Experimentation Animale, Imagine Institute, Paris, France) for attentively caring for the mice. We thank Léonard Bertrand and Elodie Dandelot for help with the graphical abstract. This study was supported by grants from AFM-Téléthon (France, project grant 16161 to M.G.-P.), INSERM (France), Université Paris Descartes (France), and Fondation ARC (France); as well as PhD fellowships from Ministère Français de la Recherche et Technologie (France, to G.S. and D.M.D.), AFM-Téléthon (France, to G.S.) and Imagine Foundation (France, to S.O.B.). This program received a state subsidy managed by the National Research Agency under the "Investments

for the Future'' program bearing the reference ANR-10-IAHU-01 and under the program ANR-10BLAN-1121-01. L.S., G.C., G.G., and M.G.-P. have a patent on GLT1 upregulation in DM1.

Received: January 15, 2017
Revised: April 27, 2017
Accepted: May 26, 2017
Published: June 27, 2017

REFERENCES

Algalarrondo, V., Wahbi, K., Sebag, F., Gourdon, G., Beldjord, C., Azibi, K., Balse, E., Coulombe, A., Fischmeister, R., Eymard, B., et al. (2015). Abnormal sodium current properties contribute to cardiac electrical and contractile dysfunction in a mouse model of myotonic dystrophy type 1. Neuromuscul. Disord. *25*, 308–320.

Angeard, N., Gargiulo, M., Jacquette, A., Radvanyi, H., Eymard, B., and Héron, D. (2007). Cognitive profile in childhood myotonic dystrophy type 1: is there a global impairment? Neuromuscul. Disord. *17*, 451–458.

Angeard, N., Jacquette, A., Gargiulo, M., Radvanyi, H., Moutier, S., Eymard, B., and Héron, D. (2011). A new window on neurocognitive dysfunction in the childhood form of myotonic dystrophy type 1 (DM1). Neuromuscul. Disord. *21*, 468–476.

Antonini, G., Soscia, F., Giubilei, F., De Carolis, A., Gragnani, F., Morino, S., Ruberto, A., and Tatarelli, R. (2006). Health-related quality of life in myotonic dystrophy type 1 and its relationship with cognitive and emotional functioning. J. Rehabil. Med. *38*, 181–185.

Bachasson, D., Moraux, A., Ollivier, G., Decostre, V., Ledoux, I., Gidaro, T., Servais, L., Behin, A., Stojkovic, T., Hébert, L.J., et al. (2016). Relationship between muscle impairments, postural stability, and gait parameters assessed with lower-trunk accelerometry in myotonic dystrophy type 1. Neuromuscul. Disord. *26*, 428–435.

Batra, R., Charizanis, K., Manchanda, M., Mohan, A., Li, M., Finn, D.J., Goodwin, M., Zhang, C., Sobczak, K., Thornton, C.A., and Swanson, M.S. (2014). Loss of MBNL leads to disruption of developmentally regulated alternative polyadenylation in RNA-mediated disease. Mol. Cell *56*, 311–322.

Bearzatto, B., Servais, L., Cheron, G., and Schiffmann, S.N. (2005). Age dependence of strain determinant on mice motor coordination. Brain Res. *1039*, 37–42.

Bearzatto, B., Servais, L., Roussel, C., Gall, D., Baba-Aïssa, F., Schurmans, S., de Kerchove d'Exaerde, A., Cheron, G., and Schiffmann, S.N. (2006). Targeted calretinin expression in granule cells of calretinin-null mice restores normal cerebellar functions. FASEB J. *20*, 380–382.

Bellamy, T.C. (2006). Interactions between Purkinje neurones and Bergmann glia. Cerebellum *5*, 116–126.

Brook, J.D., McCurrach, M.E., Harley, H.G., Buckler, A.J., Church, D., Aburatani, H., Hunter, K., Stanton, V.P., Thirion, J.P., Hudson, T., et al. (1992). Molecular basis of myotonic dystrophy: expansion of a trinucleotide (CTG) repeat at the 3′ end of a transcript encoding a protein kinase family member. Cell *68*, 799–808.

Caillet-Boudin, M.L., Fernandez-Gomez, F.J., Tran, H., Dhaenens, C.M., Buee, L., and Sergeant, N. (2014). Brain pathology in myotonic dystrophy: when tauopathy meets spliceopathy and RNAopathy. Front. Mol. Neurosci. *6*, 57.

Caliandro, P., Silvestri, G., Padua, L., Bianchi, M.L., Simbolotti, C., Russo, G., Masciullo, M., and Rossini, P.M. (2013). fNIRS evaluation during a phonemic verbal task reveals prefrontal hypometabolism in patients affected by myotonic dystrophy type 1. Clin. Neurophysiol. *124*, 2269–2276.

Charizanis, K., Lee, K.Y., Batra, R., Goodwin, M., Zhang, C., Yuan, Y., Shiue, L., Cline, M., Scotti, M.M., Xia, G., et al. (2012). Muscleblind-like 2-mediated alternative splicing in the developing brain and dysregulation in myotonic dystrophy. Neuron *75*, 437–450.

Cheron, G., Gall, D., Servais, L., Dan, B., Maex, R., and Schiffmann, S.N. (2004). Inactivation of calcium-binding protein genes induces 160 Hz oscillations in the cerebellar cortex of alert mice. J. Neurosci. *24*, 434–441.

Cheron, G., Servais, L., Wagstaff, J., and Dan, B. (2005). Fast cerebellar oscillation associated with ataxia in a mouse model of Angelman syndrome. Neuroscience *130*, 631–637.

Cheron, G., Servais, L., and Dan, B. (2008). Cerebellar network plasticity: from genes to fast oscillation. Neuroscience *153*, 1–19.

Cheron, G., Sausbier, M., Sausbier, U., Neuhuber, W., Ruth, P., Dan, B., and Servais, L. (2009). BK channels control cerebellar Purkinje and Golgi cell rhythmicity in vivo. PLoS ONE *4*, e7991.

Cheron, G., Dan, B., and Márquez-Ruiz, J. (2013). Translational approach to behavioral learning: lessons from cerebellar plasticity. Neural Plast. *2013*, 853654.

Dogan, C., De Antonio, M., Hamroun, D., Varet, H., Fabbro, M., Rougier, F., Amarof, K., Arne Bes, M.C., Bedat-Millet, A.L., Behin, A., et al. (2016). Gender as a modifying factor influencing myotonic dystrophy type 1 phenotype severity and mortality: a nationwide multiple databases cross-sectional observational study. PLoS ONE *11*, e0148264.

Gomes-Pereira, M., Foiry, L., Nicole, A., Huguet, A., Junien, C., Munnich, A., and Gourdon, G. (2007). CTG trinucleotide repeat ''big jumps'': large expansions, small mice. PLoS Genet. *3*, e52.

Goodwin, M., Mohan, A., Batra, R., Lee, K.Y., Charizanis, K., Fernández Gómez, F.J., Eddarkaoui, S., Sergeant, N., Buée, L., Kimura, T., et al. (2015). MBNL sequestration by toxic RNAs and RNA misprocessing in the myotonic dystrophy brain. Cell Rep. *12*, 1159–1168.

Hammarén, E., Kjellby-Wendt, G., Kowalski, J., and Lindberg, C. (2014). Factors of importance for dynamic balance impairment and frequency of falls in individuals with myotonic dystrophy type 1—a cross-sectional study—including reference values of Timed Up & Go, 10m walk and step test. Neuromuscul. Disord. *24*, 207–215.

Hernández-Hernández, O., Guiraud-Dogan, C., Sicot, G., Huguet, A., Luilier, S., Steidl, E., Saenger, S., Marciniak, E., Obriot, H., Chevarin, C., et al. (2013a). Myotonic dystrophy CTG expansion affects synaptic vesicle proteins, neurotransmission and mouse behaviour. Brain *136*, 957–970.

Hernández-Hernández, O., Sicot, G., Dinca, D.M., Huguet, A., Nicole, A., Buée, L., Munnich, A., Sergeant, N., Gourdon, G., and Gomes-Pereira, M. (2013b). Synaptic protein dysregulation in myotonic dystrophy type 1: disease neuropathogenesis beyond missplicing. Rare Dis. *1*, e25553.

Higashimori, H., Morel, L., Huth, J., Lindemann, L., Dulla, C., Taylor, A., Freeman, M., and Yang, Y. (2013). Astroglial FMRP-dependent translational down-regulation of mGluR5 underlies glutamate transporter GLT1 dysregulation in the fragile X mouse. Hum. Mol. Genet. *22*, 2041–2054.

Huguet, A., Medja, F., Nicole, A., Vignaud, A., Guiraud-Dogan, C., Ferry, A., Decostre, V., Hogrel, J.Y., Metzger, F., Hoeflich, A., et al. (2012). Molecular, physiological, and motor performance defects in DMSXL mice carrying >1,000 CTG repeats from the human DM1 locus. PLoS Genet. *8*, e1003043.

Kanadia, R.N., Johnstone, K.A., Mankodi, A., Lungu, C., Thornton, C.A., Esson, D., Timmers, A.M., Hauswirth, W.W., and Swanson, M.S. (2003). A muscleblind knockout model for myotonic dystrophy. Science *302*, 1978–1980.

Kanai, Y., and Hediger, M.A. (2004). The glutamate/neutral amino acid transporter family SLC1: molecular, physiological and pharmacological aspects. Pflugers Arch. *447*, 469–479.

Kim, K., Lee, S.G., Kegelman, T.P., Su, Z.Z., Das, S.K., Dash, R., Dasgupta, S., Barral, P.M., Hedvat, M., Diaz, P., et al. (2011). Role of excitatory amino acid transporter-2 (EAAT2) and glutamate in neurodegeneration: opportunities for developing novel therapeutics. J. Cell. Physiol. *226*, 2484–2493.

Kiryk, A., Aida, T., Tanaka, K., Banerjee, P., Wilczynski, G.M., Meyza, K., Knapska, E., Filipkowski, R.K., Kaczmarek, L., and Danysz, W. (2008). Behavioral characterization of GLT1 (+/−) mice as a model of mild glutamatergic hyperfunction. Neurotox. Res. *13*, 19–30.

Kong, Q., Chang, L.C., Takahashi, K., Liu, Q., Schulte, D.A., Lai, L., Ibabao, B., Lin, Y., Stouffer, N., Das Mukhopadhyay, C., et al. (2014). Small-molecule activator of glutamate transporter EAAT2 translation provides neuroprotection. J. Clin. Invest. *124*, 1255–1267.

Lin, C.L., Bristol, L.A., Jin, L., Dykes-Hoberg, M., Crawford, T., Clawson, L., and Rothstein, J.D. (1998). Aberrant RNA processing in a neurodegenerative disease: the cause for absent EAAT2, a glutamate transporter, in amyotrophic lateral sclerosis. Neuron *20*, 589–602.

Meola, G., and Sansone, V. (2007). Cerebral involvement in myotonic dystrophies. Muscle Nerve *36*, 294–306.

Minnerop, M., Weber, B., Schoene-Bake, J.C., Roeske, S., Mirbach, S., Anspach, C., Schneider-Gold, C., Betz, R.C., Helmstaedter, C., Tittgemeyer, M., et al. (2011). The brain in myotonic dystrophy 1 and 2: evidence for a predominant white matter disease. Brain *134*, 3530–3546.

Mohan, A., Goodwin, M., and Swanson, M.S. (2014). RNA-protein interactions in unstable microsatellite diseases. Brain Res. *1584*, 3–14.

Panaite, P.A., Kuntzer, T., Gourdon, G., Lobrinus, J.A., and Barakat-Walter, I. (2013). Functional and histopathological identification of the respiratory failure in a DMSXL transgenic mouse model of myotonic dystrophy. Dis. Model. Mech. *6*, 622–631.

Regan, M.R., Huang, Y.H., Kim, Y.S., Dykes-Hoberg, M.I., Jin, L., Watkins, A.M., Bergles, D.E., and Rothstein, J.D. (2007). Variations in promoter activity reveal a differential expression and physiology of glutamate transporters by glia in the developing and mature CNS. J. Neurosci. *27*, 6607–6619.

Rothstein, J.D., Patel, S., Regan, M.R., Haenggeli, C., Huang, Y.H., Bergles, D.E., Jin, L., Dykes Hoberg, M., Vidensky, S., Chung, D.S., et al. (2005). Beta-lactam antibiotics offer neuroprotection by increasing glutamate transporter expression. Nature *433*, 73–77.

Schmahmann, J.D., and Sherman, J.C. (1998). The cerebellar cognitive affective syndrome. Brain *121*, 561–579.

Schneider-Gold, C., Bellenberg, B., Prehn, C., Krogias, C., Schneider, R., Klein, J., Gold, R., and Lukas, C. (2015). Cortical and subcortical grey and white matter atrophy in myotonic dystrophies type 1 and 2 is associated with cognitive impairment, depression and daytime sleepiness. PLoS ONE *10*, e0130352.

Serra, L., Silvestri, G., Petrucci, A., Basile, B., Masciullo, M., Makovac, E., Torso, M., Spanò, B., Mastropasqua, C., Harrison, N.A., et al. (2014). Abnormal functional brain connectivity and personality traits in myotonic dystrophy type 1. JAMA Neurol. *71*, 603–611.

Serra, L., Petrucci, A., Spanò, B., Torso, M., Olivito, G., Lispi, L., Costanzi-Porrini, S., Giulietti, G., Koch, G., Giacanelli, M., et al. (2015). How genetics affects the brain to produce higher-level dysfunctions in myotonic dystrophy type 1. Funct. Neurol. *30*, 21–31.

Serra, L., Cercignani, M., Bruschini, M., Cipolotti, L., Mancini, M., Silvestri, G., Petrucci, A., Bucci, E., Antonini, G., Licchelli, L., et al. (2016). "I know that you know that I know": neural substrates associated with social cognition deficits in DM1 patients. PLoS ONE *11*, e0156901.

Servais, L., and Cheron, G. (2005). Purkinje cell rhythmicity and synchronicity during modulation of fast cerebellar oscillation. Neuroscience *134*, 1247–1259.

Servais, L., Hourez, R., Bearzatto, B., Gall, D., Schiffmann, S.N., and Cheron, G. (2007). Purkinje cell dysfunction and alteration of long-term synaptic plasticity in fetal alcohol syndrome. Proc. Natl. Acad. Sci. USA *104*, 9858–9863.

Seznec, H., Lia-Baldini, A.S., Duros, C., Fouquet, C., Lacroix, C., Hofmann-Radvanyi, H., Junien, C., and Gourdon, G. (2000). Transgenic mice carrying large human genomic sequences with expanded CTG repeat mimic closely the DM CTG repeat intergenerational and somatic instability. Hum. Mol. Genet. *9*, 1185–1194.

Seznec, H., Agbulut, O., Sergeant, N., Savouret, C., Ghestem, A., Tabti, N., Willer, J.C., Ourth, L., Duros, C., Brisson, E., et al. (2001). Mice transgenic for the human myotonic dystrophy region with expanded CTG repeats display muscular and brain abnormalities. Hum. Mol. Genet. *10*, 2717–2726.

Sicot, G., and Gomes-Pereira, M. (2013). RNA toxicity in human disease and animal models: from the uncovering of a new mechanism to the development of promising therapies. Biochim. Biophys. Acta *1832*, 1390–1409.

Sicot, G., Gourdon, G., and Gomes-Pereira, M. (2011). Myotonic dystrophy, when simple repeats reveal complex pathogenic entities: new findings and future challenges. Hum. Mol. Genet. *20* (*R2*), R116–R123.

Sistiaga, A., Urreta, I., Jodar, M., Cobo, A.M., Emparanza, J., Otaegui, D., Poza, J.J., Merino, J.J., Imaz, H., Martí-Massó, J.F., and López de Munain, A. (2010). Cognitive/personality pattern and triplet expansion size in adult myotonic dystrophy type 1 (DM1): CTG repeats, cognition and personality in DM1. Psychol. Med. *40*, 487–495.

Takado, Y., Terajima, K., Ohkubo, M., Okamoto, K., Shimohata, T., Nishizawa, M., Igarashi, H., and Nakada, T. (2015). Diffuse brain abnormalities in myotonic dystrophy type 1 detected by 3.0 T proton magnetic resonance spectroscopy. Eur. Neurol. *73*, 247–256.

Tanaka, K., Watase, K., Manabe, T., Yamada, K., Watanabe, M., Takahashi, K., Iwama, H., Nishikawa, T., Ichihara, N., Kikuchi, T., et al. (1997). Epilepsy and exacerbation of brain injury in mice lacking the glutamate transporter GLT-1. Science *276*, 1699–1702.

Theadom, A., Rodrigues, M., Roxburgh, R., Balalla, S., Higgins, C., Bhattacharjee, R., Jones, K., Krishnamurthi, R., and Feigin, V. (2014). Prevalence of muscular dystrophies: a systematic literature review. Neuroepidemiology *43*, 259–268.

Toth, A., Lovadi, E., Komoly, S., Schwarcz, A., Orsi, G., Perlaki, G., Bogner, P., Sebok, A., Kovacs, N., Pal, E., and Janszky, J. (2015). Cortical involvement during myotonia in myotonic dystrophy: an fMRI study. Acta Neurol. Scand. *132*, 65–72.

Tzingounis, A.V., and Wadiche, J.I. (2007). Glutamate transporters: confining runaway excitation by shaping synaptic transmission. Nat. Rev. Neurosci. *8*, 935–947.

Udd, B., and Krahe, R. (2012). The myotonic dystrophies: molecular, clinical, and therapeutic challenges. Lancet Neurol. *11*, 891–905.

Voogd, J., and Glickstein, M. (1998). The anatomy of the cerebellum. Trends Cogn. Sci. *2*, 307–313.

Wang, E.T., Cody, N.A., Jog, S., Biancolella, M., Wang, T.T., Treacy, D.J., Luo, S., Schroth, G.P., Housman, D.E., Reddy, S., et al. (2012). Transcriptome-wide regulation of pre-mRNA splicing and mRNA localization by muscleblind proteins. Cell *150*, 710–724.

Weber, Y.G., Roebling, R., Kassubek, J., Hoffmann, S., Rosenbohm, A., Wolf, M., Steinbach, P., Jurkat-Rott, K., Walter, H., Reske, S.N., et al. (2010). Comparative analysis of brain structure, metabolism, and cognition in myotonic dystrophy 1 and 2. Neurology *74*, 1108–1117.

Wiles, C.M., Busse, M.E., Sampson, C.M., Rogers, M.T., Fenton-May, J., and van Deursen, R. (2006). Falls and stumbles in myotonic dystrophy. J. Neurol. Neurosurg. Psychiatry *77*, 393–396.

Wozniak, J.R., Mueller, B.A., Lim, K.O., Hemmy, L.S., and Day, J.W. (2014). Tractography reveals diffuse white matter abnormalities in myotonic dystrophy type 1. J. Neurol. Sci. *341*, 73–78.

Cell Reports, Volume *19*

Supplemental Information

Downregulation of the Glial GLT1 Glutamate Transporter and Purkinje Cell Dysfunction in a Mouse Model of Myotonic Dystrophy

Géraldine Sicot, Laurent Servais, Diana M. Dinca, Axelle Leroy, Cynthia Prigogine, Fadia Medja, Sandra O. Braz, Aline Huguet-Lachon, Cerina Chhuon, Annie Nicole, Noëmy Gueriba, Ruan Oliveira, Bernard Dan, Denis Furling, Maurice S. Swanson, Ida Chiara Guerrera, Guy Cheron, Geneviève Gourdon, and Mário Gomes-Pereira

SUPPLEMENTAL TABLES

Table S1. Clinical data of control individuals (related to Figure 4).

	Non-DM controls			
	a	**b**	**c**	**d**
Sex	M	M	M	M
Diagnosis	N/A,	Charcot-Marie-Tooth Disease;	Rheumathoide arthritis	Limb-girdle muscular dystrophy
Neuropsychological profile	N/D	N/D	N/D	N/D
Neuroimaging	N/D	N/D	N/D	N/D
Age; cause of death	79; *Pneumocystis* pneumonia	71; pneumonia	76; interstitial pneumonia	66; cardiac failure

Table S2. Clinical data of DM1 individuals (related to Figure 4).

	DM1 samples						
	e	**f**	**g**	**h**	**i**	**j**	**k**
Sex	**F**	**F**	**F**	**M**	**F**	**M**	**M**
CTGs in blood (age of analysis)	1300-1400 (40)	>2500 (N/D)	N/D	N/D	1730 (73)	700-1100 (30)	1600-1800 (40)
CTGs in cerebellum (age of analysis)	400 (69)	450 (64)	200 (62)	500 (58)	350 (73)	350 (67)	400 (62)
Age of onset	40	Unknown	54	46	40	30	40
Clinical form of DM	Adult DM1	N/D	Late onset DM1	Adult DM1	Adult DM1	Adult DM1	Adult DM1
DM main symptoms	Gait problems	Gait problems	Cardiac arrhythmia; gait problems	Limb muscle weakness	Muscle weakness and atrophy in all extremities	Gait problems	Gait problems
Neuropsychological profile	WAIS-R (VIQ74, PIQ73, IQ73)	N/D	N/D	N/D	Memory loss	N/D	N/D
Neuroimaging	Diffuse atrophy	General brain atrophy	N/D	N/D	Bilateral fronto-temporal atrophy	N/D	Normal
Age; cause of death	69; pneumonia	64; ARDS	62; pneumonia	58; pneumonia	73; pneumonia	67; pneumonia	62; heart failure

ARDS, acute respiratory distress syndrome; N/A not applicable; N/D, not determined.

Table S3. Primary antibodies for immunofluorescence and immunohistochemistry (related to Figures 1 and 4).

Antigene	Supplier; vendor reference; RRID	Species origin	Blocking and incubation conditions	Ab dilution
CALB1	Swant; CB38; AB_10000340	mouse	10% NGS, 1h, RT	1/400
FOX1	Abcam; ab83574; AB_1859807	mouse	10% NGS, 1h, RT	1/400
FOX2	Abcam; ab57154; AB_2285090	mouse	10% NGS, 1h, RT	1/400
GFAP	DakoCytomation; Z0334; AB_10013382	rabbit	10% NGS, 1h, RT	1/400
GLAST	Abcam; ab416; AB_304334	rabbit	10% NGS, 1h, RT	1/200
GLT1	Alomone; AGC-022; AB_2039891	rabbit	10% NGS, 1h, RT	1/200
MBNL1	MB1A from Glen Morris (gift)	mouse	0.1% BSA, 10% NGS, 1H, RT	1/10
MBNL2	MB2A from Glen Morris (gift)	mouse	0.1% BSA, 10% NGS, 1h, RT	1/10
NeuN	Chemicon; MAB377; AB_2298772	mouse	10% NGS, 1h, RT	1/400
Ubiquitin	Dako Cytomation; Z0458; AB_2315524	rabbit	10% NSS, 1h, RT	1/500

BSA, bovine serum albumin; NGS, normal-goat serum; NSS, normal swine serum; RT, room temperature.

Table S4. Oligonucleotide primers sequences for RT-PCR analysis of laser micro-dissected mouse cells (related to Figure 1).

Gene	Exon	Primer 1	Primer 2	Primer 3	PCR product size (bp)
Calb1	N/A	GTGCTTTGGGTGACAGTCCT	TGAGCTGGATGCTTTGCTGA	TGGATTTCCCCGAAAATCTACCA	139
Glast	N/A	GGGGAGCACAAATCTGGTGA	CCGTGCCTGGATCTGTGAAT	GTAACCCGGAAGAACCCCTG	159
Mbnl1	7	CAATGTTGGTCACGGGGAATC	GCTGCCCAATACCAGGTCAAC	TGGTGGGAGAAATGCTGTATGC	270/216
Mbnl2	5	CCATAGGGACAAATGCGG	ACCGTAACCGTTTGTATGGATTAC	TTGGTAAGGGATGAAGAGC	255/201

N/A, not applicable.

Table S5. Oligonucleotide primer sequences for mouse and human RT-PCR analysis (related to Figure 1).

Gene	Species	Exon	Forward primer	Reverse primer	PCR product size (bp)
18S	Mouse	qRT-PCR	CAGTGAAACTGCGAATGG	CGGGTTGGTTTTGATCTG	165
18S	Human	qRT-PCR	CAGTGAAACTGCGAATGG	CGGGTTGGTTTTGATCTG	165
Fabp7	Mouse	qRT-PCR	TACATGAAAGCTCTGGGCGTG	TGTCCGGATCACCACTTTGC	105
Glt1	Mouse	Whole transcript	CCGTTAAATACCGCTCTCCGC	GCTGGGGAGTTTATTCAAGAATTG	1854
Glt1	Mouse	13	TGCTGGAACTTTGCCTGTTACC	GTGTTGGGAGTCAATGGTGTCC	433/298
Glt1	Mouse	Intron 11	TCATCGCCATCAAGGACTTAGAAG	GCTGGGAATACTGGCTGC GAGAGAAACAGGAAGCAGCAAATG	-In11: 434 +In 11: 266
Glt1	Mouse	qRT-PCR	TGGACTGGCTGCTGGATAGA	CGGTGTTGGGAGTCAATGGT	118
GLT1	Human	Whole transcript	ACCGTCCTCTGCCACCACTCT	ACGCTGGGGAGTTTATTCAAGAAT	2194
GLT1	Human	12	TTTGCCTGTCACCTTTCGTTG	TTAGAGTTGCTTTCCCTGTGGTTC	504/369
GLT1	Human	Intron 10	GGCAACTGGGGATGTACA	ACGCTGGGGAGTTTATTCAAGAAT CCAGAAGGCTCAGAAGT	-In10: 835 +In10: 345
GLT1	Human	qRT-PCR	TAGCCGCCATCTTTATAGCCC	CGGCTGTCAGAATGAGGAGC	150
MAPT/ TAU	Human	10	CTGAAGCACCAGCCAGGAGG	TGGTCTGTCTTGGCTTTGGC	367/274
Mbnl1	Mouse	7	TGGTGGGAGAAATGCTGTATGC	GCTGCCCAATACCAGGTCAAC	270/216
MBNL1	Human	7	TGGTGGGAGAAATGCTGTATGC	GCTGCCCAATACCAGGTCAAC	270/216
Mbnl2	Mouse	5	CTTTGGTAAGGGATGAAGAGCAC	ACCGTAACCGTTTGTATGGATTAC	255/201
MBNL2	Human	5	CTTTGGTAAGGGATGAAGAGCAC	ACCGTAACCGTTTGTATGGATTAC	255/201
Sept4	Mouse	qRT-PCR	GGTGGCAGGAGAATCTGGTC	CCGATCCCGGTACAAGTCAG	76
β-ACTIN	Human	N/A	CCGTCTTCCCCTCCATCG	CCTCGTCGCCCACATAGG	87
Tbp1	Mouse	N/A	GGTGTGCACAGGAGCCAAGAGTG	AGCTACTGAACTGCTGGTGGGTC	192
TBP1	Human	N/A	GGTGTGCACAGGAGCCAAGAGTG	AGCTACTGAACTGCTGGTGGGTC	192

qRT-PCR, quantitative RT-PCR; -In10, intron 10 exclusion; +in10, intron 10 inclusion; -In11, intron 11 exclusion; +in11, intron 11 inclusion; N/A, not applicable.

Table S6. Primary antibodies for western blot immunodetection (related to Figure 3, 4, 5 and 6).

Antigene	Supplier; vendor reference; RRID	PAGE (%)	Species origin	Blocking and incubation conditions	Ab dilution
Actin	BD Biosciences; 612656; AB_2289199	10-12	mouse	5% blotto, 1h, RT	1/5,000
CALB1	Swant; cb38; AB_10000340	12	rabbit	5% blotto, 1h, RT	1/500,000
CALB2	Abcam; ab1550; AB_90764	12	rabbit	5% blotto, 1h, RT	1/5,000
CELF1	Millipore; 05-621; AB_309851	10	mouse	5% blotto, 1h, RT	1/1,000
CELF2	Sigma; C9367; AB_1078584	10	mouse	5% blotto, 2h, RT	1/1,000
GAPDH	Genetex; GTX627408; AB_11174761	10-12	mouse	5% blotto, 1h, RT	1/10,000
GLAST	Abcam; ab416; AB_304334	10	rabbit	5% blotto, 1h, RT	1/5,000
GLT1	Alomone; AGC-022; AB_2039891	10	rabbit	5% blotto, 1h, RT	1/1,000
GLUR2	Abcam; ab206293; N/A	10	rabbit	5% blotto, 1h, RT	1/2000
NMDAR1	ThermoFisher Scientific; 32-0500; AB_2533060	10	mouse	5% blotto, 1h, RT	1/500
PSD95	Abcam; ab2723; AB_303248	10	mouse	5% blotto, 1h, RT	1/1000
PVALB	Millipore; MAB1572; AB_2174013	12	mouse	2.5 BSA, 1h, RT	1/500

N/A, not applicable; RT, room temperature.

Table S7. Sequences of MBNL1 and MBNL2 shRNA (related to Figure 5).

Gene	Sequence	Complementary sequence
MBNL1	AACACGGAAUGUAAAUUUGCA TT	UGCAAAUUUACAUUCCGUGUUTT
MBNL2	CACCGUAACCGUUUGUAUTT	CAUACAAACGGUUACGGUTT

SUPPLEMENTAL FIGURES

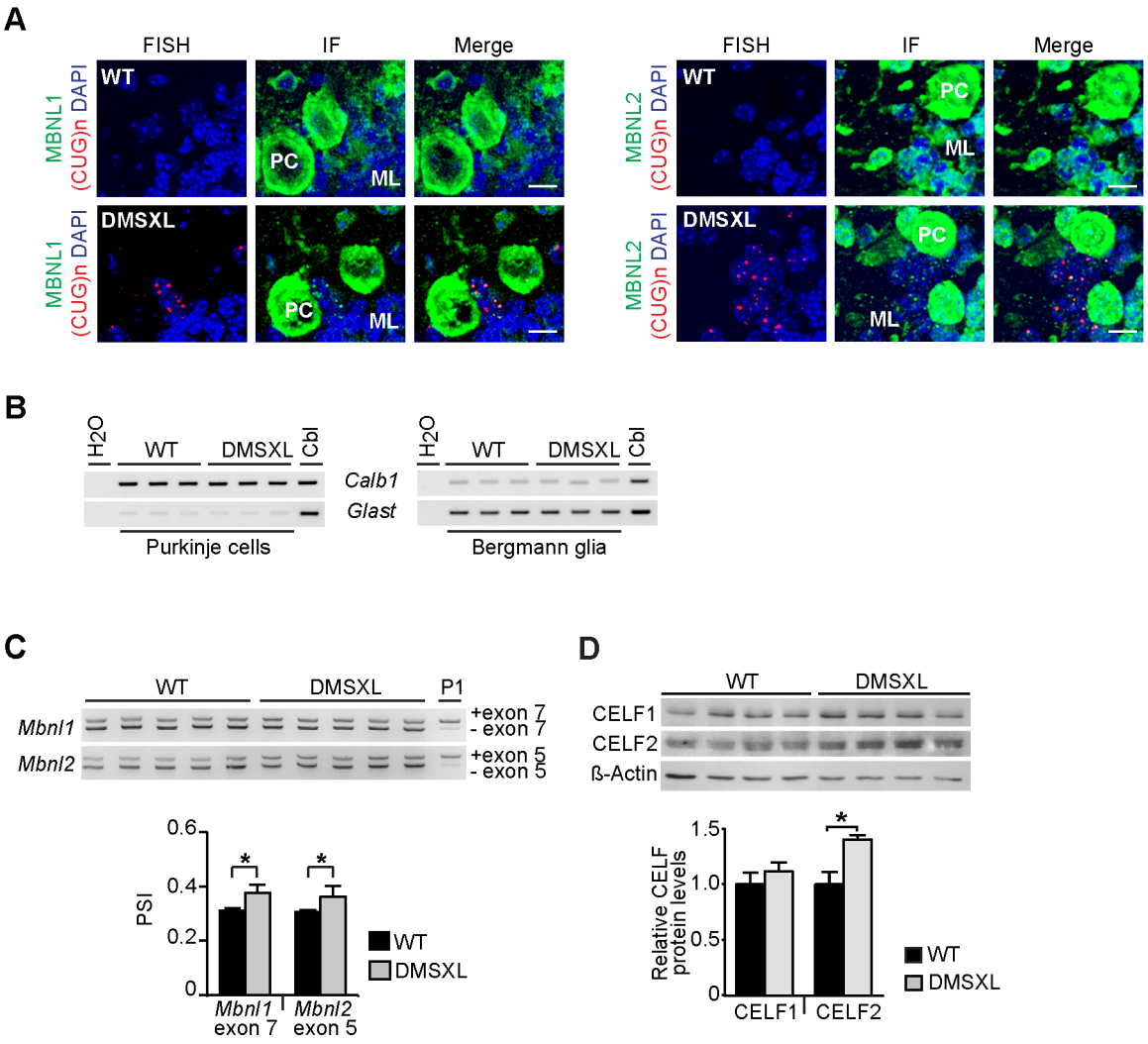

Figure S1. RNA foci, splicing and CELF protein levels in DMSXL cerebellum (related to Figure 1). (A) FISH detection of RNA foci (red) and immunofluorescence of MBNL1 and MBNL2 (green) in WT and DMSXL mouse cerebellum. The scale bar represents 10 µm. PC, Purkinje cells; ML, molecular layer. **(B)** RT-PCR expression analysis of RNA transcripts primarily expressed in Purkinje cells (calbindin 1, *Calb1*) and in Bergmann glia (*Glast*), to confirm the nature of the cells collected by laser cell microdissection from the cerebellum of WT and DMSXL mice (n=3 animals, each genotype). *Calb1* transcripts were found predominantly in collected Purkinje cells, while *Glast* showed higher expression in microdissected Bergmann astrocytes. H_2O, no DNA control; Cbl, mouse cerebellum tissue control. **(C)** RT-PCR analysis of splicing profiles of *Mbnl1* and *Mbnl2* mRNA transcripts in the cerebellum of 2-month-old DMSXL and WT mice (n=5, each genotype) and in WT newborn animals (P1, pool of 3 animals). The graphs represent the mean PSI (±SEM) of alternative exons. **(D)** To determine the contribution of CELF protein dysregulation to missplicing, we quantified CELF1 and CELF2 levels in whole cerebellum by western blot (n=4, each genotype). The graphs represent the mean (±SEM) relative to normalized WT controls. Only CELF2 was significantly upregulated in DMSXL mice. ß-Actin was used as internal control. **P*<0.05; Mann-Whitney U test.

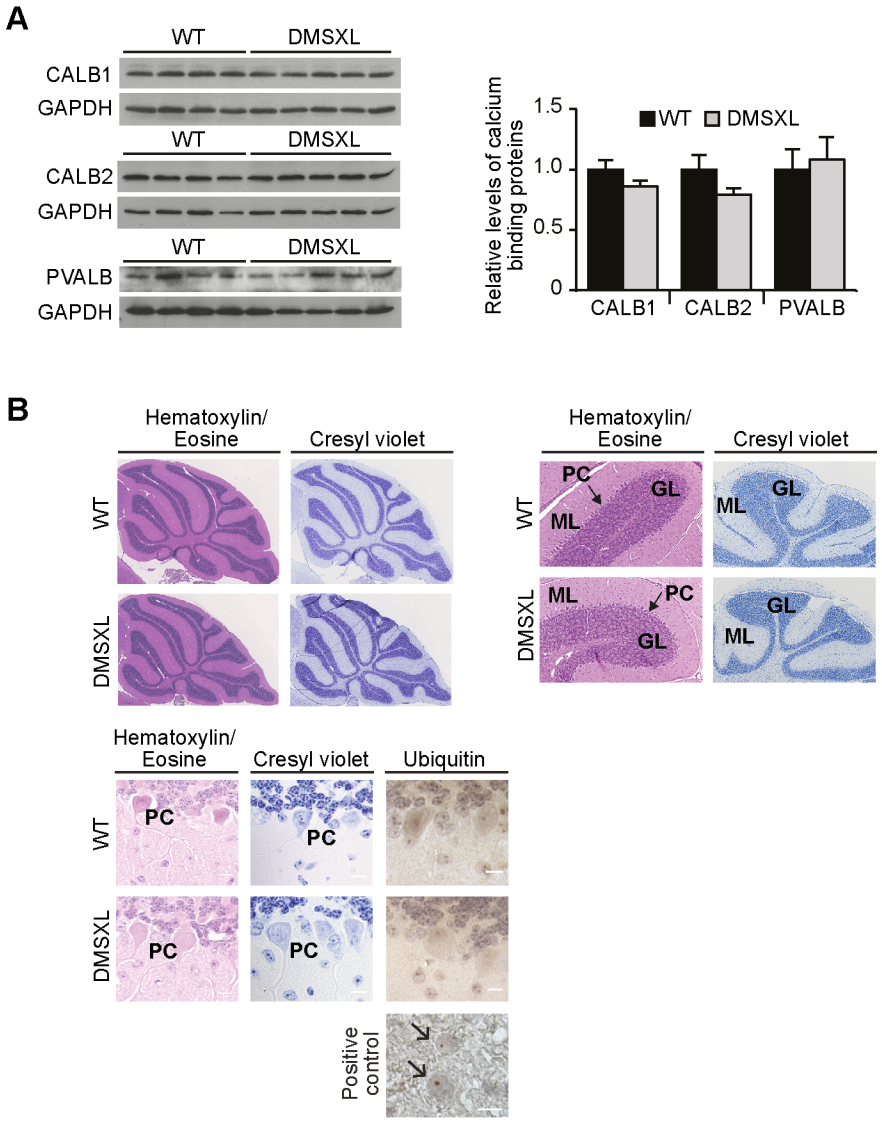

Figure S2. Expression of calcium-binding proteins is not altered in DMSXL cerebellum (related to Figure 2). (A) Western blot analysis of key calcium-buffering proteins (calbindin 1, CALB1; calbindin 2/calretinin, CALB2; and parvalbumin, PVALB) in the cerebellum of DMSXL mice (n=5), relative to WT controls (n=4). The graphs represent average protein levels (±SEM), relative to normalized WT controls. GAPDH was used as loading control. No significant difference was found in protein levels in DMSXL cerebellum. **(B)** Signs of neurodegeneration and histopathology in DMSXL cerebellum were investigated by standard hematoxylin-eosin and cresyl violet staining. Proteotoxicity was studied by the immunodetection of ubiquitin aggregates. Lower magnification pictures (top panels) do not show evidence of overall changes in cerebellum structure, morphology or cell density in DMSXL mice. Higher magnification pictures (bottom panels) do not reveal obvious changes in cell morphology, neurodegeneration or ongoing protein stress. FXTAS knock-in mouse brains were used as positive controls for the accumulation of ubiquitin-containing protein aggregates. PC, Purkinje cell; GL, granular layer; ML, molecular layer.

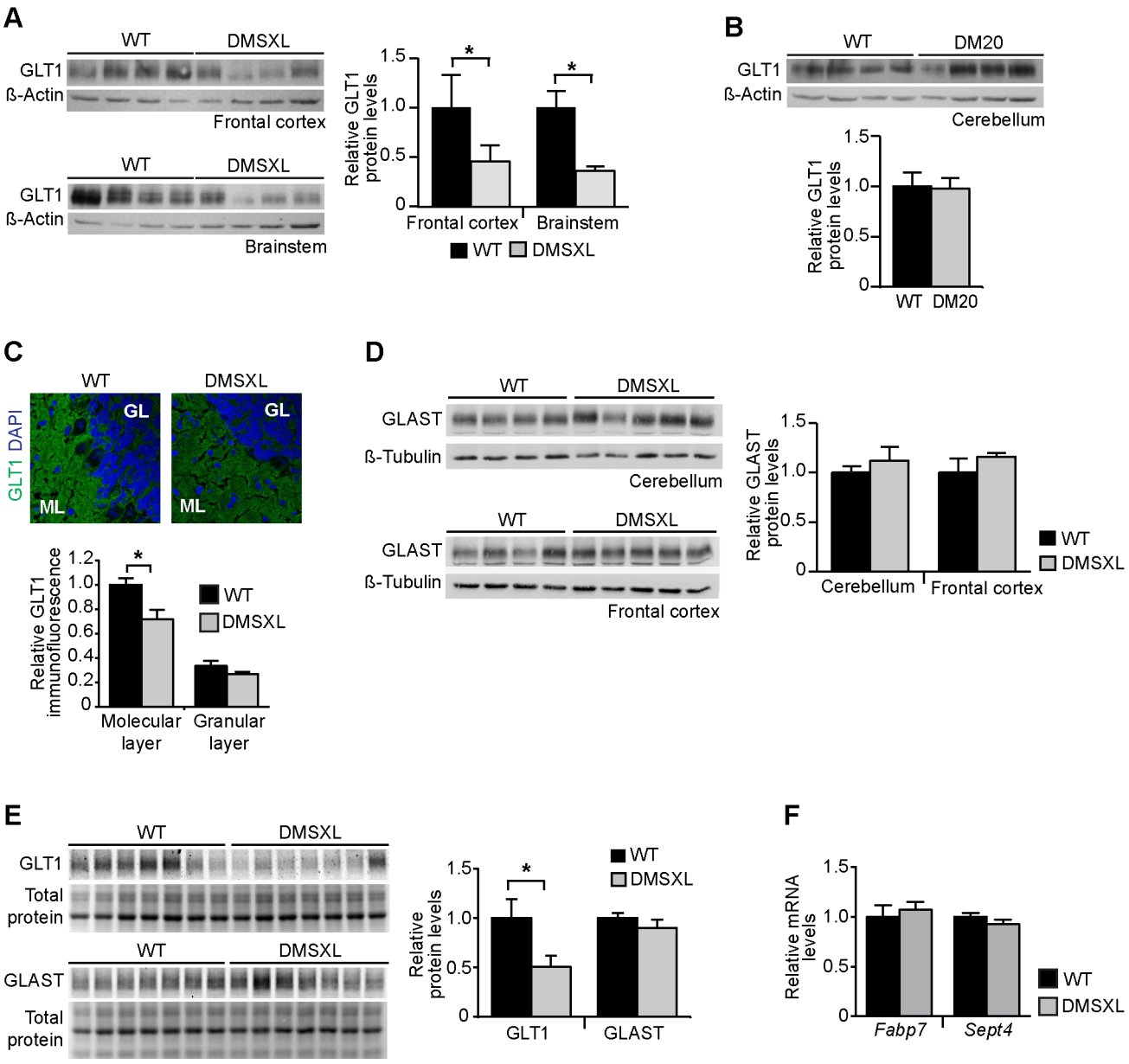

Figure S3. **GLT1 is downregulated in multiple brain regions of DMSXL mice (related to Figure 3). (A)** To assess the extent of GLT1 downregulation, we quantified GLT1 protein levels in additional brain regions from 2-month-old mice by western blot. GLT1 protein was significantly downregulated in the frontal cortex and brainstem of DMSXL mice, compared to WT controls (n=4, each genotype). ß-Actin was used as loading control. **(B)** Quantification of GLT1 protein levels in control DM20 transgenic mice, relative to WT littermates (n=4, each genotype). Overexpression of short *DMPK* transcripts is not sufficient to affect GLT1 steady-state levels. **(C)** Semi-quantitative analysis of GLT1 immunofluorescence (±SEM) in the molecular and granular layers in the cerebellum of two-month-old DMSXL and WT mice. Representative pictures of three independent analyses. The same camera acquisition settings were used for both images. **(D)** Western blot analysis of GLAST protein expression in the cerebellum and frontal cortex of DMSXL (n=5) and WT mice (n=4). ß-Tubulin was used as loading control. **(E)** Quantification of GLT1 and GLAST protein steady-state levels in DMSXL and WT primary astrocytes (n=7, each genotype). Representative western blot analysis of three technical replicates. Total protein was visualized by stain-free protocols and used as loading control. GLT1 show a significant 50% reduction in DMSXL primary astrocytes, while GLAST protein levels remain unchanged. **(F)** Quantification of Bergmann-specific *Fabp7* and *Sept4* transcripts in the cerebellum of DMSXL and WT mice (n=6, each group). Graphs represent the mean ± SEM. **P*<0.05, Mann-Whitney U test.

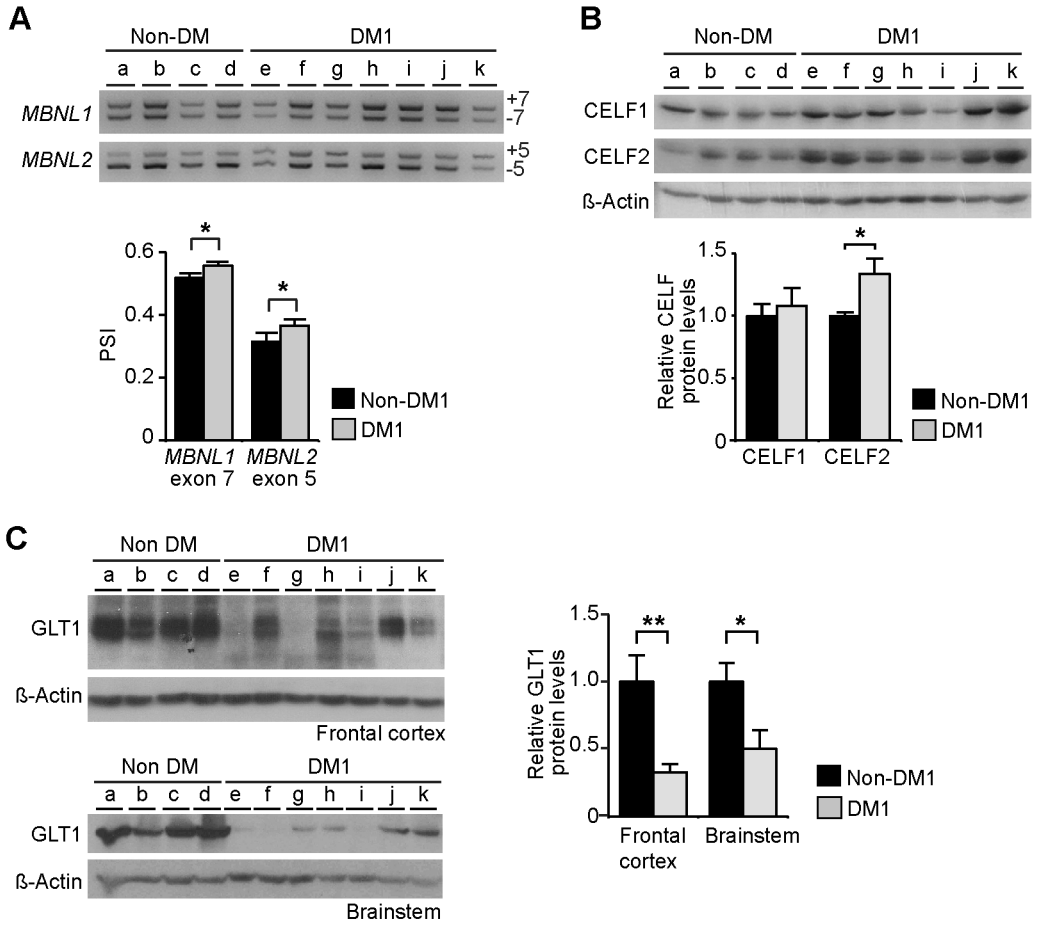

Figure S4. RNA splicing and GLT1 protein levels in human DM1 brains (related to Figure 4). (A) RT-PCR analysis of *MBNL1* exon 7 and *MBNL1* exon 5 in human cerebellum tissue samples in adult DM1 patients (n=7), relative to non-DM controls (n=4). The graphs represent the mean PSI (±SEM) of the alternative exons studied. **(B)** Quantification of CELF1 and CELF2 proteins by western blot in the cerebellum of DM1 patients (n=7), relative to non-DM controls (n=4), revealed significant upregulation of CELF2, to an extent similar to DMSXL mice. ß-Actin was used as loading control. **(C)** Western blot analysis of GLT1 steady-state levels in the frontal cortex and brainstem of adult DM1 patients and non-DM controls. GLT1 is significantly downregulated in DM1 frontal cortex and brainstem. ß-Actin was used as loading control **P*<0.05, ***P*<0.01; Mann-Whitney U test.

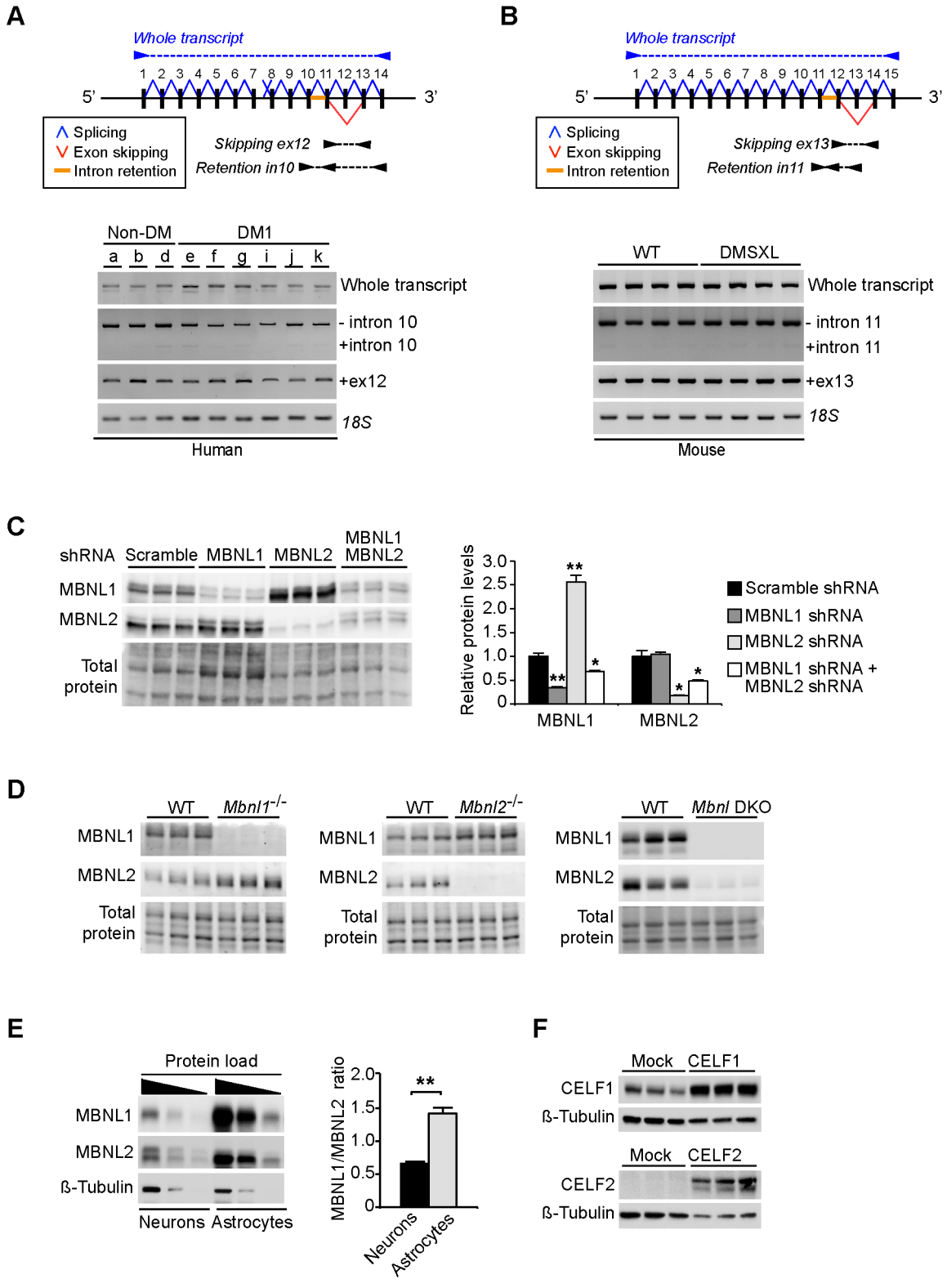
A
Whole transcript
1 2 3 4 5 6 7 8 9 10 11 12 13 14
5'
3'
Splicing
Exon skipping
Intron retention
Skipping ex12
Retention in10
Non-DM
DM1
a b d e f g i j k
Whole transcript
- intron 10
+intron 10
+ex12
18S
Human
B
Whole transcript
1 2 3 4 5 6 7 8 9 10 11 12 13 14 15
5'
3'
Splicing
Exon skipping
Intron retention
Skipping ex13
Retention in11
WT
DMSXL
Whole transcript
- intron 11
+intron 11
+ex13
18S
Mouse
C
shRNA
Scramble
MBNL1
MBNL2
MBNL1 MBNL2
MBNL1
MBNL2
Total protein
Relative protein levels
3.0
2.5
2.0
1.5
1.0
0.5
0
**
**
*
*
*
MBNL1
MBNL2
Scramble shRNA
MBNL1 shRNA
MBNL2 shRNA
MBNL1 shRNA + MBNL2 shRNA
D
WT
Mbnl1-/-
MBNL1
MBNL2
Total protein
WT
Mbnl2-/-
MBNL1
MBNL2
Total protein
WT
Mbnl DKO
MBNL1
MBNL2
Total protein
E
Protein load
MBNL1
MBNL2
ß-Tubulin
Neurons
Astrocytes
MBNL1/MBNL2 ratio
2.0
1.5
1.0
0.5
0
**
Neurons
Astrocytes
F
Mock
CELF1
CELF1
ß-Tubulin
Mock
CELF2
CELF2
ß-Tubulin

Figure S5. GLT1 downregulation is not associated with splicing abnormalities and is mediated by MBNL1 inactivation (related to Figure 5). (A) RT-PCR analysis of full-length *GLT1* mRNA, alternative exons and intron inclusion in human brains. The top illustration represents the human *GLT1* gene with 14 exons and shows the alternative splicing events studied. The arrowheads represent the location of the oligonucleotide primers used in the splicing analysis of whole transcript, skipping of exon 12 and inclusion intron 10. The results revealed no obvious differences between DM1 (n=6) and non-DM cerebella (n=3). **(B)** RT-PCR analysis of full-length *Glt1* mRNA, alternative exon 13 and intron 11 inclusion in the cerebellum of 2-month-old mice. The location of oligonucleotide primers (arrowheads) is indicated on the mouse gene. DMSXL cerebellum did not show obvious missplicing events, compared to WT controls (n=4, each genotype). **(C)** MBNL1 and MBNL2 detection by western blot following knocking down of these proteins by shRNA in T98G cells. Total protein was visualized by stain-free protocols and used as loading control. The graphs represent average protein levels (±SEM) relative to normalized scramble shRNA controls. MBNL1 was decreased down to 34% in cells transfected with MBNL1 shRNA. MBNL2 shRNA-treated cells showed MBNL2 protein levels down to 18% of scramble controls, but a 155% compensatory increase of MBNL1. MBNL1 and MBNL2 double knocking-down was more modest that individual strategies, resulting in protein levels that were 69% and 48% of those in scramble controls, respectively. **(D)** Western blot expression analysis of MBNL1 and MBNL2 proteins *Mbnl1*$^{-/-}$, *Mbnl2*$^{-/-}$ and *Mbnl* double knock out (DKO) mice, and in WT littermate controls (n=3, each genotype). Mice were aged 3-4 months. Total protein was visualized by stain-free protocols and used as loading control. **(E)** Western blot detection and quantification of MBNL1 and MBNL2 protein levels in primary neurons and astrocytes. Decreasing amounts of a protein pool of whole cell lysate from three WT cultures were electrophoresed and immunodetected. Both MBNL1 and MBNL2 proteins are more abundant in astrocytes. The graph represents the MBNL1/MBNL2 expression ratio in each cell type (mean ± SEM), and shows that MBNL1 relative expression is twofold higher in mouse primary astrocytes than in neurons. ß-Tubulin was used as loading control. **(F)** Western blot immunoblotting showing CELF1 and CELF2 upregulation in T98G cells transfected with expressing vectors. ß–Tubulin was used as loading control. **P*<0.05, ***P*<0.01; one-way ANOVA in (C) and Mann-Whitney U test in (E).

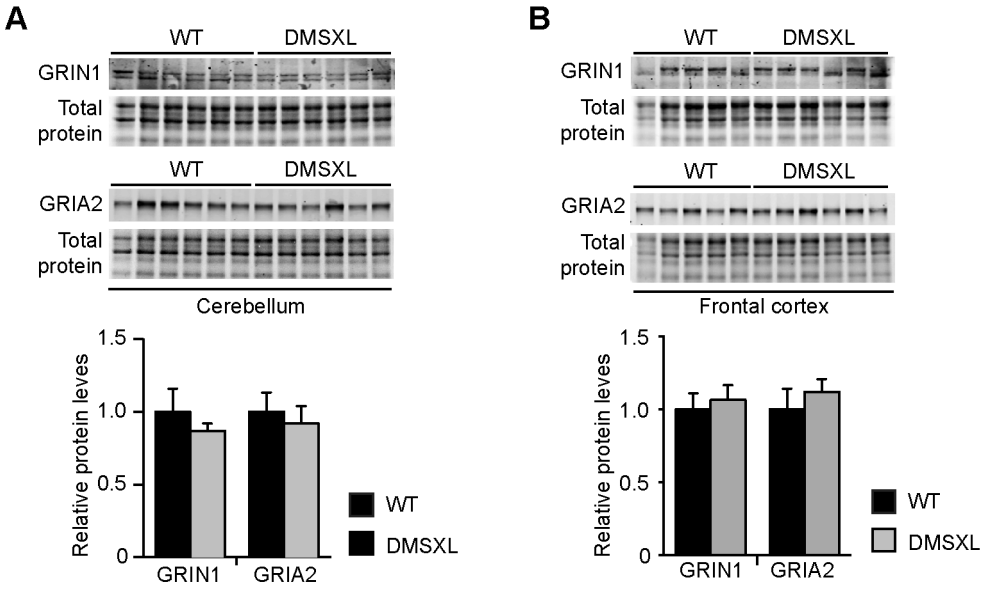

Figure S6. Glutamate receptor expression in mouse brain tissue (related to Figure 6). Quantification of GRIN1 and GRIA2 glutamate receptor subunits in the **(A)** cerebellum and **(B)** frontal cortex of 2-month-old DMSXL and WT controls (n=5-6, each genotype). Representative western blots of three technical replicates. Total protein was visualized by stain-free protocols and used as loading control. The graphs represent the mean (±SEM) relative protein levels, normalized to WT controls, and show no significant differences in the expression of glutamate receptors in DMSXL brain tissue.

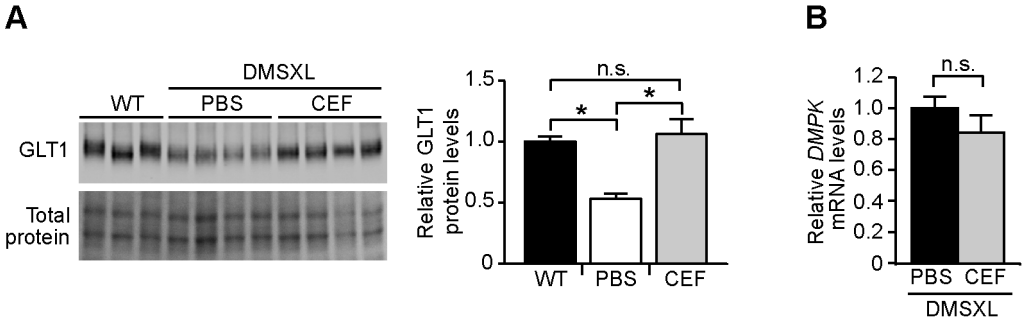

Figure S7. Ceftriaxone upregulates GLT1 but does not change *DMPK* transcript levels in DMSXL mice (related to Figure 7). (A) We confirmed that ceftriaxone increased GLT1 in DMSXL mice to levels undistinguishable from those detected in WT controls. Representative western blot analysis of GLT1 levels in the cerebellum of 2-month-old DMSXL mice following PBS or ceftriaxone treatment (200 mg/kg, daily i.p. injections, over 5 consecutive days) (n=4, each treatment group). WT controls are also shown (n=3). Total protein was visualized by stain-free protocols and used as loading control. The graph represents the mean levels of GLT1 protein (±SEM) in the cerebellum of DMSXL mice injected with ceftriaxone, PBS and in WT controls. **(B)** Real-time PCR quantification of expanded *DMPK* transcripts in the cerebellum of DMSXL mice treated with ceftriaxone (n=6) or PBS (n=6) showed no effect of the antibiotic on transgene expression. **P*<0.05, one-way ANOVA in (A); n.s. not statistically significant, Mann-Whitney U test in (B).

SUPPLEMENTAL EXPERIMENTAL PROCEDURES AND METHODS

Mouse genotyping.
Mouse experiments were performed with wild-type controls of the same litter to reduce inter-individual variability. DMSXL transgenic mice were generated and genotyped as previously described (Gomes-Pereira et al., 2007; Hernandez-Hernandez et al., 2013). All DMSXL mice used for this work were adult (2-4 months) homozygotes, unless stated otherwise. The control DM20 line expresses non-pathogenic 20-CTG tracts (Seznec et al., 2001; Seznec et al., 2000). *Glt1* knock-out mice on C57BL/6 background (Tanaka et al., 1997) were provided by Prof. Niels Christian Danbolt (University of Oslo, Norway). The *Glt1* transgenic status was determined by multiplex PCR of tail DNA, using P1-GLT1 (5'-GGGTTGTAGATGTGTAGAGATGG-3'), P2-GLT1 (5'-CCTGACAGAGATCAGAGCACGT-3') and P3-GLT1 (5'-ATTCGCAGCGCATCGCCTTCTA-3') oligonucleotide primers. *Glt1* wild-type alleles generate a 469-bp product, while the disrupted allele generates a 210-bp allele.

Fluorescent in situ hybridization (FISH).
Ribonuclear inclusions were detected with a 5'-Cy3-labelled (CAG)5 PNA probe, as previously described (Huguet et al., 2012). Immunofluorescence (IF) combined with fluorescent *in situ* hybridization (FISH) was performed as previously described (Hernandez-Hernandez et al., 2013). Antibody references and working dilutions are listed in **Table S3**.

Laser Capture Microdissection (LCM).
Purkinje cells and surrounding cells were individually microdissected from one to two-month-old DMSXL and wild-type control mouse cerebellum, using a Palm Micro Beam (Carl Zeiss). RNA extraction, cDNA synthesis and RT-PCR analysis of candidate genes performed as previously described (Peixoto et al., 2004). Average of 100 Purkinje cells and 300 surrounding cells were separately collected in triplicate from three DMSXL mice and from three wild-type control mice. For each cDNA sample, three replicates of the RT-PCR reactions were performed. The sequences of the oligonucleotide primers used in the RT-PCR analysis of Purkinje and Bergmann cells laser microdissected from DMSXL cerebellum are listed in **Table S4**.

RT-PCR analysis of alternative splicing.
Total RNA was extracted from half mouse cerebellum collected 2-month-old mice, following tissue homogenization with stainless steel beads, and using a TRIZOL extraction protocol combined with a commercially available RNA Purification Kit, as previously described (Huguet et al., 2012). cDNA synthesis, semi-quantitative RT-PCR analysis of alternative splicing and qRT-PCR quantification of *DMPK* transcripts were performed as described elsewhere (Gomes-Pereira et al., 2007; Hernandez-Hernandez et al., 2013), using oligonucleotide primers listed in **Tables S5**. All samples were normalized to TATA-binding protein (Tbp) or ß-actin. The Percent of Spliced In (PSI) was used to quantify the splicing level of alternative exons: PSI = (intensity of inclusion isoform) / (intensity of inclusion isoform + intensity of exclusion isoform) x 100.

Western blot analysis.
Total protein was extracted from 20-30 mg brain tissue dissected from 2-month-old mice, using RIPA buffer (ThermoFisher Scientific; 89901), supplemented with 0.05% CHAPS (Sigma; C3023), 1x complete protease inhibitors (Roche; 04693124001), 1x Phospho STOP phosphatase inhibitors (Roche; 04693124001). Protein concentrations in the supernatants were determined using a Bio-Rad DCTM protein assay (Bio-Rad; 500-0114). Protein integrity was checked by Coomassie stain of a 10% SDS-polyacrylamide gel. Volumes corresponding to 30-60 µg of protein were mixed with Laemmli sample buffer and boiled for 5 min. Proteins were resolved in 10% or 12% SDS-polyacrylamide gels and transferred onto PVDF membranes. Following Ponceau red staining to verify the efficiency of protein transfer, membranes were blocked in 1X TBS-T (10 mM Tris-HCl, 0.15 M NaCl, 0.05% Tween 20) containing blotto (Santa Cruz Biotech; sc2325) and incubated overnight at 4°C with the corresponding primary antibody. After three washes with 1X TBS-T, membranes were incubated at room temperature during 1 h with the appropriated HRP-secondary antibody. Primary antibody references, working dilutions and blocking conditions are indicated in **Table S6**. After washing with 1X TBS-T, antibody binding was visualized by chemiluminiscence (PerkinElmer). Densitometric analysis with Quantity One® 1D Analysis Software (Bio-Rad) has been performed to quantify signal intensity. Quantitative western blot results are represented as means of steady-state levels (±SEM) in transgenic animals, relative to normalized controls. Total protein electrophoresed through thialo-containing polyacrylamide gels (Bio-Rad) was visualized under UV light.

Electrophysiological and behavioral assessment.
In vivo electrophysiological study in alert mice. Two-month old DMSXL and control mice were surgically prepared for chronic recording of neuronal activity in the cerebellum. The experimental session for extracellular recording of Purkinje cells (PCs) activity and local field potential (LFP) analysis in the cerebellar cortex was performed as previously described

(Cheron et al., 2004). The strength of the rhythmicity was quantified with a rhythm index (Cheron et al., 2004; Sugihara and Furukawa, 1995).
The runway test. Motor coordination was examined by the runway test as previously described (Servais and Cheron, 2005). In this test, 3-4 month old DMSXL (n=20) and control (n=21) mice, male and females included, ran along an elevated runway with low obstacles intended to impede progress. The runway was 100 cm long and 0.7 cm width. Obstacles being of 1 cm diameter wood rod and 0.7 cm width were placed every 10 cm along the runway. Mice were placed on one extremity of the runway and had to move along the runway to reach the other end. The number of slips of the right hind leg was counted. Each mouse underwent four consecutive trials per day during 5 consecutive days. The test was repeated following a test-free period of three weeks, over one day (four consecutive trials), to assess the learning capacity of mice.

iTraq proteomics analysis.
The analysis of mouse brain proteome by isobaric tagging for relative and absolute quantifications (iTRAQ) mass spectrometry was performed on individual DMSXL and wild-type male mice, aged 2 months (n=4 per genotype, for whole cell proteins extracts; n=2 for membrane bound protein fraction). Membrane-bound protein fractions were purified from mouse cerebellum, as previously described (Cox and Emili, 2006).
iTraq labeling. Protein iTRAQ labeling was performed according to the manufacturer's instructions (iTRAQ 4plex kit, ABSCIEX). Briefly, protein pellets (100 µg) were suspended in 20 µL of 500 mM triethylammonium bicarbonate (TEAB) and 1 µL of 2% SDS, they were then reduced with 2 µL of 50 mM tris-(2-carboxyethyl) phosphine (TCEP) for 1h at 60°C and finally alkylated with 1 µL of 200 mM methyl methanethiosulfonate (MMTS) for 10 min at room temperature. Proteins were digested with 2 µg of sequencing grade modified trypsin (Promega) for 16h at 37°C. The resulted peptides were labeled with iTRAQ reagents and quenched with Milli-Q water. The labeled samples were mixed in a 1:1:1:1 ratio and stored at -20°C.
Sample clean-up by SCX & Sep-Pak. An aliquot of the iTRAQ 4-plex-labeled peptide mixture (100 µg) was cleaned up with a cation-exchange cartridge SCX (from ICAT Reagent Kit, ABSCIEX), equilibrated with 10 mM potassium phosphate, pH 3, 25% acetonitrile. Peptides were eluted with 500 µL of 350 mM potassium chloride, 25% acetonitrile and concentrated in a centrifugal evaporator, under vacuum. The sample was reconstituted in 0.1% trifluoroacetic acid and loaded on a Sep-Pak cartridge (Waters) for desalting. After washing, the peptides were eluted in 1 mL of 70% acetonitrile- 0.1% trifluoroacetic acid and dried in a vacuum concentrator.
MS/MS Analysis. Nano-LC-MS/MS analysis was performed on an Ultimate 3,000 Rapid Separation Liquid Chromatography (RSLC) system (Dionex) coupled to LTQ-Orbitrap Velos mass spectrometer (Thermo Scientific). Dried peptides were resuspended in 0.1% (v/v) trifluoroacetic acid, 10% acetonitrile, and pre-concentrated on a 75 µm i.d. reversed-phase (RP) trapping column and separated with an aqueous-organic gradient (solution "A": 0.1% formic acid in 5% acetonitrile; solution "B": 0.085% formic acid in 80% (acetonitrile; flow rate 400 nl/min) on a 75 µm RP column (Acclaim PepMap RSLC 75 µm x 15 cm, 2 µm, 100Å, Dionex). Samples were eluted using a linear gradient from 5% to 40% solvent B in 190 min. One FTMS full scan was performed (resolution 60,000; positive polarity; centroid data; scan range 400 to 2,000 m/z) and the 10 most intense signals were subjected to MS/MS fragmentation both in the collision-induced dissociation (CID) cell and high-energy collision dissociation (HCD) cell for the same precursor ion. CID fragmentation was performed with a target value of 5000, collision energy of 35 V, Q value of 0.25 and activation time of 10 ms while HCD was done using a target value of 50,000, collision energy of 50 V and activation time of 0.1 ms. LC-MS/MS data were transferred to the Proteome Discoverer software v1.2 to create the .mgf file, which was searched against the *Mus musculus* subset (16547 sequences) of the UniprotKB/Swissprot database (release 2012_06; 536796 sequences) using the Mascot search engine (version 2.2.07; Matrix Science) for protein identification and protein quantification. Fixed modification (iTRAQ 4plex (K) and N-terminus) and variable modification (Methylthio (C), Oxidation (M)) were allowed as well as one missed cleavage. Monoisotopic peptide mass tolerance was ± 5 ppm (after linear recalibration), and fragment mass tolerance was ± 0.5 Da. Filters for protein quantification were set as follow: protein ratio type was "weighted", normalization was done with summed intensities and outliers were removed automatically. Only proteins quantified with at least 2 peptides and with the ion score higher than 25 were retained. False discovery rate was less than 2%. Differences between the DMSXL and WT proteomes were evaluated by a Mann-Whitney U test ($P<0.05$), as previously described (Jeanson et al., 2014). To determine the most deregulated proteins, the standard deviation of the protein ratios was calculated for each experiment, and the Gaussian distributions were normalized. An average threshold was calculated to determine the most upregulated proteins (last 20% on the right of the Gaussian) and the most downregulated proteins (first 20% on the left of the Gaussian).
GO enrichment analysis. Gene Ontology (GO) enrichment analysis of differently expressed proteins was performed using the functional annotation tool Database for Annotation, Visualization and Integrated Discovery (DAVID) v.6.7 (http://david.abcc.ncifcrf.go) (Huang da et al., 2009). GO enrichment analysis integrated the information of the cellular components and biological processes associated with the deregulated proteins, to provide a list biological terms organized into classes of related genes/proteins. Significant GO terms were identified at a FDR <0.05.

Fluorescence quantification of GLT1
Confocal images of WT and DMSXL slices of cerebellum stained on the same glass slide were acquired as z-stacks at the 40x magnification with a Leica TSC SP8 SMD Confocal microscope, using the same laser power and PMT values. Z projections were analyzed using Fiji software (Schindelin et al., 2012) by drawing the granular and molecular layer and measuring the integrated density of the regions of interest.

Tissue fractioning for western blot analysis
Cytosolic and membrane-bound protein were prepared by serial centrifugation of tissue homogenates collected from the cerebellum of 2-month-old mice, in isotonic sucrose solution, as previously described (Nishida et al., 2004). The enrichment for cytosolic and cell membrane proteins was confirmed by immunodetection of GAPDH and PSD95, respectively.

Glutamate uptake
Uptake of radioactive glutamate by cultured astrocytes was performed using published methods (Beaule et al., 2009) and expressed as fmol of radioactive glutamate per µg of total protein. Glutamate transporter inhibitors were added to the medium, to inhibit total glutamate transporter (50 µM TBOA; Bio-Techne, 10/1/2532), GLT1-mediated glutamate transport (200 nM WAY-213613; Santa Cruz Biotechnology, sc-203720) or GLAST-mediated glutamate transport (5 µM UCPH 101; Santa Cruz Biotechnology, sc-361391)

Fluorescent assay of glutamate neurotoxicity in neuroglial co-cultures
The co-cultures of neurons and astrocytes were established as previously described (Kaech and Banker, 2006). Briefly, the astrocytes were purified from the frontal cortex of P1 mouse embryos and cultured for two weeks in DMEM low glucose (31885-023Life Technologies, 31885-023), supplemented with 10% FBS and 0.05 mg/ml gentamycin (Life Technologies; 15710). E16.5 mouse neurons were dissociated from embryonic frontal cortex in a mixture of trypsin/DNase I and plated in Neurobasal-A medium (Life Technologies, 10888022), supplemented with 1X B27 supplement (Life Technologies, 17504044), 0.5 mM L-Glutamine (Life Technologies, 25030024), 1% antibiotic and antimycotic (Life Technologies, 15240-096) and 5% FBS. The primary neurons from the WT and DMSXL mice and were infected with NeuroLight^{RM} red lentivirus (Essen BioScience, 4584), encoding the mKate2 fluorescent protein under the Synapsin-1 Promoter (MOI=3) four hours after plating in serum free neuronal medium. The next day neurons were washed with Neurobasal medium to remove the lentivirus and primary astrocytes, cultured two weeks, were plated on top of neurons. Neuronal fluorescence was monitored by live cell video-microscopy (IncuCyte Live Cell Analysis System, Essen BioScience), by acquiring phase contrast and red fluorescent images each hour, using the Neurotrack module of acquisition and measurement of neurite extension. On day 8 of the mixed cultures, 50 µM of glutamate were added to the medium and neurite collapse monitored for 12-24 hours. If used, glutamate receptor antagonists were also added on day 8, together with glutamate (10 µM CNQX, antagonist of AMPA receptors, Abcam, ab120017; 10 µM (+)-MK 801 maleate, antagonist of NMDA receptors, Abcam, ab144485). The rate of neurite collapse was expressed as mm of length change, per mm^2 of surface studied, per day. For the rescuing assays, GLT1 was upregulated 30 hours prior to the assessment of glutamate neurotoxicity, either by transfection of GLT1-GFP-expressing plasmids (provided by Dr. Nicolas Reyes, Institute Pasteur, Paris, France) or by treating co-cultures with 10 µM ceftriaxone.

Plasmid and shRNA transfection.
Cultured cells were transfected with 250 ng/mL to 1.25 µg/mL of plasmid DNA using JetPrime transfection reagent and protocol (PolyPlus, 114-75). shRNA was transfected at a final concentration of 200 nM using Lipofectamine RNAiMax reagent and protocol (Life Technologies; 13778150). shRNA sequences are shown in the **Table S7**.

Ceftriaxone treatment.
Mouse intraperitoneal injections of ceftriaxone (Sigma; C5793) in PBS (20 µg/µl) were performed through a 27G needle to a final dose of 200 mg/kg. Male and female mice were injected at 2 months of age, daily over a period of five days, prior to molecular, electrophysiological and behavioral assessment. Daily injections of ceftriaxone continued during motor assessment in the runway test. Treatment control mice were injected with PBS (n=5 per group, including male and females).

Microscope and images processing.
Images were taken with a fluorescent microscope Zeiss ApoTome 2 or with a Leica TSC SP8 SMD Confocal microscope. Images were treated with ImageJ software (Schneider et al., 2012).

Statistical analysis.
Statistical analyses were performed with Prism (GraphPad Software, Inc), SPSS (v14.0, SPSS Inc©), Statistica (v6.0, StaatSoft®) and/or Excel software. When two groups were compared, we first performed a normality test. Parametric data were compared using a two-tailed Student's t-test (with equal or unequal variance, as appropriate). Non-parametric data were compared using a two-tailed Mann-Whitney U test. For one-way ANOVA, if statistical significance was achieved, we performed post-test analysis to account for multiple comparisons. Statistical significance was set at $P<0.05$. The data are presented as mean ± standard error of the mean (±SEM).

SUPPLEMENTAL REFERENCES

Beaule, C., Swanstrom, A., Leone, M.J., and Herzog, E.D. (2009). Circadian modulation of gene expression, but not glutamate uptake, in mouse and rat cortical astrocytes. PLoS One *4*, e7476.

Cheron, G., Gall, D., Servais, L., Dan, B., Maex, R., and Schiffmann, S.N. (2004). Inactivation of calcium-binding protein genes induces 160 Hz oscillations in the cerebellar cortex of alert mice. J Neurosci *24*, 434-441.

Cox, B., and Emili, A. (2006). Tissue subcellular fractionation and protein extraction for use in mass-spectrometry-based proteomics. Nat Protoc *1*, 1872-1878.

Gomes-Pereira, M., Foiry, L., Nicole, A., Huguet, A., Junien, C., Munnich, A., and Gourdon, G. (2007). CTG trinucleotide repeat "big jumps": large expansions, small mice. PLoS Genet *3*, e52.

Hernandez-Hernandez, O., Guiraud-Dogan, C., Sicot, G., Huguet, A., Luilier, S., Steidl, E., Saenger, S., Marciniak, E., Obriot, H., Chevarin, C.*, et al.* (2013). Myotonic dystrophy CTG expansion affects synaptic vesicle proteins, neurotransmission and mouse behaviour. Brain *136*, 957-970.

Huang da, W., Sherman, B.T., and Lempicki, R.A. (2009). Systematic and integrative analysis of large gene lists using DAVID bioinformatics resources. Nat Protoc *4*, 44-57.

Huguet, A., Medja, F., Nicole, A., Vignaud, A., Guiraud-Dogan, C., Ferry, A., Decostre, V., Hogrel, J.Y., Metzger, F., Hoeflich, A.*, et al.* (2012). Molecular, physiological, and motor performance defects in DMSXL mice carrying >1,000 CTG repeats from the human DM1 locus. PLoS Genet *8*, e1003043.

Jeanson, L., Guerrera, I.C., Papon, J.F., Chhuon, C., Zadigue, P., Pruliere-Escabasse, V., Amselem, S., Escudier, E., Coste, A., and Edelman, A. (2014). Proteomic analysis of nasal epithelial cells from cystic fibrosis patients. PLoS One *9*, e108671.

Kaech, S., and Banker, G. (2006). Culturing hippocampal neurons. Nat Protoc *1*, 2406-2415.

Nishida, A., Iwata, H., Kudo, Y., Kobayashi, T., Matsuoka, Y., Kanai, Y., and Endou, H. (2004). Nicergoline enhances glutamate uptake via glutamate transporters in rat cortical synaptosomes. Biol Pharm Bull *27*, 817-820.

Peixoto, A., Monteiro, M., Rocha, B., and Veiga-Fernandes, H. (2004). Quantification of multiple gene expression in individual cells. Genome research *14*, 1938-1947.

Schindelin, J., Arganda-Carreras, I., Frise, E., Kaynig, V., Longair, M., Pietzsch, T., Preibisch, S., Rueden, C., Saalfeld, S., Schmid, B.*, et al.* (2012). Fiji: an open-source platform for biological-image analysis. Nat Methods *9*, 676-682.

Schneider, C.A., Rasband, W.S., and Eliceiri, K.W. (2012). NIH Image to ImageJ: 25 years of image analysis. Nat Methods *9*, 671-675.

Servais, L., and Cheron, G. (2005). Purkinje cell rhythmicity and synchronicity during modulation of fast cerebellar oscillation. Neuroscience *134*, 1247-1259.

Seznec, H., Agbulut, O., Sergeant, N., Savouret, C., Ghestem, A., Tabti, N., Willer, J.C., Ourth, L., Duros, C., Brisson, E.*, et al.* (2001). Mice transgenic for the human myotonic dystrophy region with expanded CTG repeats display muscular and brain abnormalities. Hum Mol Genet *10*, 2717-2726.

Seznec, H., Lia-Baldini, A.S., Duros, C., Fouquet, C., Lacroix, C., Hofmann-Radvanyi, H., Junien, C., and Gourdon, G. (2000). Transgenic mice carrying large human genomic sequences with expanded CTG repeat mimic closely the DM CTG repeat intergenerational and somatic instability. Hum Mol Genet *9*, 1185-1194.

Sugihara, I., and Furukawa, T. (1995). Potassium currents underlying the oscillatory response in hair cells of the goldfish sacculus. J Physiol *489 (Pt 2)*, 443-453.

Tanaka, K., Watase, K., Manabe, T., Yamada, K., Watanabe, M., Takahashi, K., Iwama, H., Nishikawa, T., Ichihara, N., Kikuchi, T.*, et al.* (1997). Epilepsy and exacerbation of brain injury in mice lacking the glutamate transporter GLT-1. Science *276*, 1699-1702.